The Journal of Experimental Biology 216, 2548-2563

doi:10.1242/jeb.081802

RESEARCH ARTICLE

Cardiovascular design in fin whales: high-stiffness arteries protect against adverse pressure gradients at depth

M. A. Lillie[1,*], M. A. Piscitelli[1], A. W. Vogl[2], J. M. Gosline[1] and R. E. Shadwick[1]

[1]Department of Zoology and [2]Department of Cellular and Physiological Sciences, University of British Columbia, Vancouver, BC, Canada, V6T 1Z4

*Author for correspondence (lillie@zoology.ubc.ca)

SUMMARY

Fin whales have an incompliant aorta, which, we hypothesize, represents an adaptation to large, depth-induced variations in arterial transmural pressures. We hypothesize these variations arise from a limited ability of tissues to respond to rapid changes in ambient ocean pressures during a dive. We tested this hypothesis by measuring arterial mechanics experimentally and modelling arterial transmural pressures mathematically. The mechanical properties of mammalian arteries reflect the physiological loads they experience, so we examined a wide range of fin whale arteries. All arteries had abundant adventitial collagen that was usually recruited at very low stretches and inflation pressures (2–3 kPa), making arterial diameter largely independent of transmural pressure. Arteries withstood significant negative transmural pressures (−7 to −50 kPa) before collapsing. Collapse was resisted by recruitment of adventitial collagen at very low stretches. These findings are compatible with the hypothesis of depth-induced variation of arterial transmural pressure. Because transmural pressures depend on thoracic pressures, we modelled the thorax of a diving fin whale to assess the likelihood of significant variation in transmural pressures. The model predicted that deformation of the thorax body wall and diaphragm could not always equalize thoracic and ambient pressures because of asymmetrical conditions on dive descent and ascent. Redistribution of blood could partially compensate for asymmetrical conditions, but inertial and viscoelastic lag necessarily limits tissue response rates. Without pressure equilibrium, particularly when ambient pressures change rapidly, internal pressure gradients will develop and expose arteries to transient pressure fluctuations, but with minimal hemodynamic consequence due to their low compliance.

Key words: artery, diving, fin whale, thoracic pressure.

Received 19 October 2012; Accepted 28 February 2013

INTRODUCTION

In comparison to the aorta of a terrestrial mammal, fin whales (*Balaenoptera physalus* Linnaeus 1758) are reported to have an unusually compliant aortic arch coupled to an unusually incompliant aorta (Shadwick and Gosline, 1994). In terrestrial mammals, compliance is distributed along the aorta, but in some diving mammals it appears concentrated in the arch (Shadwick and Gosline, 1995), an adaptation that maintains arterial flow during the protracted diastole of bradycardia by giving the aorta the properties of a Windkessel (Drabek, 1975; Drabek and Burns, 2002; Mottishaw et al., 1999; Shadwick and Gosline, 1995). Such coupling of a compliant arch with a stiff aorta has been observed in harbour (*Phoca vitulina*) and Weddell seals (*Leptonychotes weddellii*) (Rhode et al., 1986), but the fin whale represents a more extreme separation of properties, with the thoracic aorta 30 times stiffer than the arch (Shadwick and Gosline, 1994). The stiffness of the fin whale thoracic aorta was attributed to its unusually high collagen content (Gosline and Shadwick, 1996). Collagen is stiff, and in a terrestrial mammalian artery it is slack at low blood pressures but straightens and becomes taut around physiological pressures to prevent possible over-inflation at higher pressures (Armentano et al., 1991; Bank et al., 1996; Cox, 1978; Lillie et al., 2012). Delaying collagen recruitment for loading until physiological pressures optimizes the mechanical performance of arteries. The fin whale aorta deviates from the terrestrial model by stiffening at what is believed to be below physiological pressures, affording little compliance at physiological pressures. This difference raises the possibility that these whales are exposed to a different pattern of arterial pressures during a dive. Terrestrial mammals can maintain a narrow range of transmural blood pressures – the pressure inside an artery minus the pressure outside – in part because the extravascular pressure remains essentially constant around the atmospheric pressure of 101 kPa. Controlling transmural pressures may be more difficult in a diving whale, where ambient ocean pressures increase by 101 kPa every 10 m depth.

This paper explores the possibility that removing compliance from the thoracic aorta represents an adaptation to depth-induced variations in arterial transmural pressure. During a dive, ambient ocean pressures change rapidly and substantially, and the ability of the tissues to respond to these pressures will differ in the thoracic and extra-thoracic compartments. Most tissues outside the thorax are largely incompressible and so deform little despite direct exposure to ambient ocean pressures. In this study we assume the extravascular pressure in these extra-thoracic regions, $P_{\mathrm{extrathor}}$, is close to ambient. The extravascular pressures inside the thorax, P_{thor}, are affected by structures unique to that compartment – the air-filled lungs, which require significant deformation to be pressurized, and the ribs, which make the required deformation more difficult to achieve. Extravascular pressures may therefore differ between the thoracic and extra-thoracic compartments, and that could affect arterial transmural pressures.

The average pressure inside a cetacean artery is set in the thorax as the extravascular thoracic pressure plus the cardiac overpressure, represented here by the mean value of 13 kPa based on a terrestrial mammal. The mean transmural pressure for an artery within the thorax is therefore $P_{thor} + 13 - P_{thor}$, and so should vary with cardiac overpressure but remain independent of P_{thor}. The mean transmural pressure for an artery outside the thorax is $P_{thor} + 13 - P_{extrathor}$ and therefore depends on both the cardiac overpressure and on any difference between P_{thor} and $P_{extrathor}$. Depth-induced changes in transmural pressure could substantially exceed the normal variations associated with the cardiac pulse, and should $P_{extrathor}$ exceed P_{thor} by more than 13 kPa, the arteries outside the thorax would be exposed to a net negative pressure and could be subject to collapse. Thus the transmural pressure of arteries outside the thorax may change with depth due to differing compliances of the thoracic and extrathoracic compartments.

Additionally, transmural pressures may change with time. The preceding argument is based on equilibrium, but with descent rates exceeding $5\,\mathrm{m\,s^{-1}}$ (Goldbogen et al., 2006) ambient pressures can increase by over $50\,\mathrm{kPa\,s^{-1}}$, making equilibrium difficult or impossible to attain. The tissue's response rate, limited by its inertia and viscoelasticity, may be inadequate to prevent pressure gradients from developing, and pressure transients could enter the arterial system if depth-induced changes in intra-arterial pressures simply lead or lag extravascular pressures.

Thus, we identify two factors central to the performance of a fin whale artery during a dive: (1) whether arterial compliance varies with transmural pressure, and (2) whether transmural pressures vary with depth or time. If arterial properties vary but transmural pressures remain essentially constant, the whale arterial system could function as it does in terrestrial mammals. If both properties and pressures vary, then the arterial response should change with depth, with significant hemodynamic consequences. If properties are constant [due to early collagen recruitment at low pressures and consequent high stiffness (low compliance)], then the arterial response would be independent of and so tolerant of any variation in transmural pressure. The studies by Gosline and Shadwick (Gosline and Shadwick, 1996; Shadwick and Gosline, 1994) were restricted to the aorta and carotid artery, and it is not known whether the unusual mechanical responses continue along the arterial tree to smaller vessels. Based on their studies, we hypothesized that fin whale arteries experience depth-induced variations in arterial transmural pressures, in part due to differences in extravascular pressures inside and outside the thorax (P_{thor} and $P_{extrathor}$), and in part due to a time delay transmitting pressures throughout the thorax, but that any hemodynamic consequences of these pressures are minimized by early collagen recruitment in all arteries.

We tested this hypothesis in two parts: first, we measured arterial compliance experimentally, and second, we modelled arterial transmural pressures mathematically. The focus of the experimental part was to establish whether arterial compliance varied with transmural pressure. We examined the morphology and *in vitro* mechanical properties of a range of fin whale arteries exposed to both positive and negative transmural pressures. We included arteries from the thoracic rete – a massive plexus of anastomosing arteries that occupies the extrapleural space along the dorsal thoracic wall. It has been hypothesized that these arteries engorge with blood at depth, providing a volume capacitance that offsets air volume loss from lung collapse and helps equilibrate pressures inside and outside the thorax (Barnett et al., 1958; Walmsley, 1938). We have excluded craniospinal arteries, which are encased in bone and so are not directly exposed to ambient pressures. We found that the inflation response of all but one of the arteries tested was essentially independent of pressure. The focus of the theoretical part was to establish the likelihood that transmural pressures vary with depth or time, and this was done by modelling the diving response of a fin whale thorax. Model inputs were thorax morphology and ambient ocean pressures at various depths. From these parameters we calculated the volume changes required to equalize thorax pressures with ambient pressure at depth and the resultant forces developed in thoracic wall in achieving these volume changes. Model outputs were the optimal mechanical stiffness of the thorax wall necessary for equalization of thorax pressures with ambient pressures, and the pressure gradients that would result from suboptimal thorax stiffness. The model predicted that thorax mechanical stiffness would be suboptimal at least part of the time because of inherent differences in conditions during descent and ascent coupled with insufficient tissue response times. As a result, depth-induced variations in transmural pressures are likely to occur, but these variations should be tolerable because of the pressure-independent response of the arteries.

MATERIALS AND METHODS

Animals

Arteries were collected from fresh fin whale carcasses as part of a commercial whaling operation at Hvalfjörður, Iceland during the summers of 2009 and 2010. The whales were cooled at sea by running seawater through the aorta and delivered to the station within 8 to 24 h of death. Tissues were either tested fresh at the station or frozen and imported to Canada under Convention on International Trade in Endangered Species of Wild Fauna and Flora (CITES) permits.

Histology

Histological sections were made from unpressurized, formalin-fixed samples and stained with hematoxylin and eosin or Verhoeff's elastica van Gieson. Additional sections were prepared from cryosections of unfixed tissue and examined under polarized light to examine collagen birefringence.

Artery inflation tests

Arteries were tested at ambient temperature (~15–20°C). Small and medium-sized arteries were tested in 0.9% saline and large arteries in tap water. Arteries were mounted on PVC tubing or hypodermic needles and tested untethered, with one end attached to either a pressure reservoir or tap water supply. Pressures were monitored with a pressure transducer. Arteries were conditioned by approximately five inflation cycles to around 20 kPa over 1 to 2 min. Images were then collected at regular intervals using a 12 megapixel camera to obtain outer diameter (OD) and outer radius, r_o. Fiducial marks along the vessel were used to measure local segment lengths of the unloaded artery, L, and loaded artery, l. At the end of the inflation test some arteries were tested for collapse (see below), and all arteries were ultimately cut transversely and photographed wet in air. Images were digitized with ImageJ (National Institutes of Health, Bethesda, MD, USA) to obtain the outer and inner radii of the unloaded artery, R_o and R_i, respectively.

The inner radius in the pressurized vessel, r_i, was calculated as:

$$r_i = \sqrt{r_o^2 - (R_o^2 - R_i^2)L/l}\,, \tag{1}$$

assuming constant wall volume. The midwall radius r_{mid} was the average of r_i and r_o. Stretch ratios for the circumferential, λ_θ, and axial directions, λ_z, were calculated as:

$$\lambda_\theta = \frac{r_{mid}}{R_{mid}}\,, \tag{2}$$

and

$$\lambda_z = \frac{l}{L}. \quad (3)$$

For comparison, inflation tests were run on 12 pig thoracic aortas following the protocol of Lillie et al. (Lillie et al., 2012).

Artery uniaxial tests

Two whale arterial rings and one pig thoracic aortic ring were mounted on parallel bars and subjected to a varying uniaxial load, F. Photographs were taken at each load increment. Circumferential stretch ratio, λ_θ, was measured from fiducial markers on the outer wall. Stress, σ_θ, was calculated as:

$$\sigma_\theta = \frac{F\lambda_\theta}{2w(R_o - R_i)}, \quad (4)$$

where w is the unloaded ring width. Deformation was calculated as Green strain, ε_θ:

$$\varepsilon_\theta = 0.5(\lambda_\theta^2 - 1). \quad (5)$$

Green strain is nonlinear strain measure containing higher order terms that is used where deformations are large. For small deformations, the quadratic term becomes negligible and the Green strain then approximates engineering strain (Humphrey and DeLange, 2004). Circumferential secant modulus, E_θ, is a measure of wall stiffness and was defined as:

$$E_\theta = \frac{\sigma_\theta}{\varepsilon_\theta}. \quad (6)$$

Artery collapse tests

We determined the negative transmural pressure $P_{collapse}$ required to cause buckling and collapse of an artery held horizontally and submerged in saline or water. One end of the artery was open to surrounding saline and the other was attached to a 6 m long saline-filled Tygon tube (ID 10 mm). The other end of the tube was initially positioned 5 m below the level of the artery. When the tube end was open to the atmosphere the saline column generated a sufficiently large negative pressure to collapse the arterial wall and allow only a minimal outflow of saline from the tube end. The end of the tube was then gradually raised, reducing the negative pressure, until the artery returned to its normal shape, which was marked by a substantial increase in outflow. The point at which the flow changed from minimal to high was the collapse point, and the pressure at that point, $P_{collapse}$, was determined from the height of the artery above the open tube end. In preliminary tests we found that the effect of axial stretch on $P_{collapse}$ was small, as has been previously reported (Bertram, 1987), and therefore tested the arteries without an imposed axial stretch.

RESULTS

Tissue morphology and histology

Arteries were collected from the thorax and head, generally following the branches of the aortic arch as far as possible. Collagen was prominent and abundant in the adventitia and perivascular tissue in all arteries examined, as illustrated by the internal thoracic artery in Fig. 1. Fig. 1A shows taut collagen fibres on the outside of an internal thoracic artery inflated to 21 kPa pressure, and Fig. 1B a histological section of the same artery with collagen visible in the adventitia and perivascular tissue. The structure of the internal thoracic artery was that of a muscular artery. The media was largely circumferential smooth muscle cells and devoid of lamellar or fibrous elastin. The inner portion of the adventitia contained fibroblasts throughout a remarkably thick layer of external elastic lamellae alternating with collagen (Fig. 2). In the longitudinal section shown in Fig. 2 and in a cross-section of the same vessel (not shown), the elastin runs both parallel and perpendicular to the cut surface, suggesting the lamellae are discontinuous or fibrous rather than sheet-like. The outer adventitial portion contained dense collagen bundles (Fig. 1A).

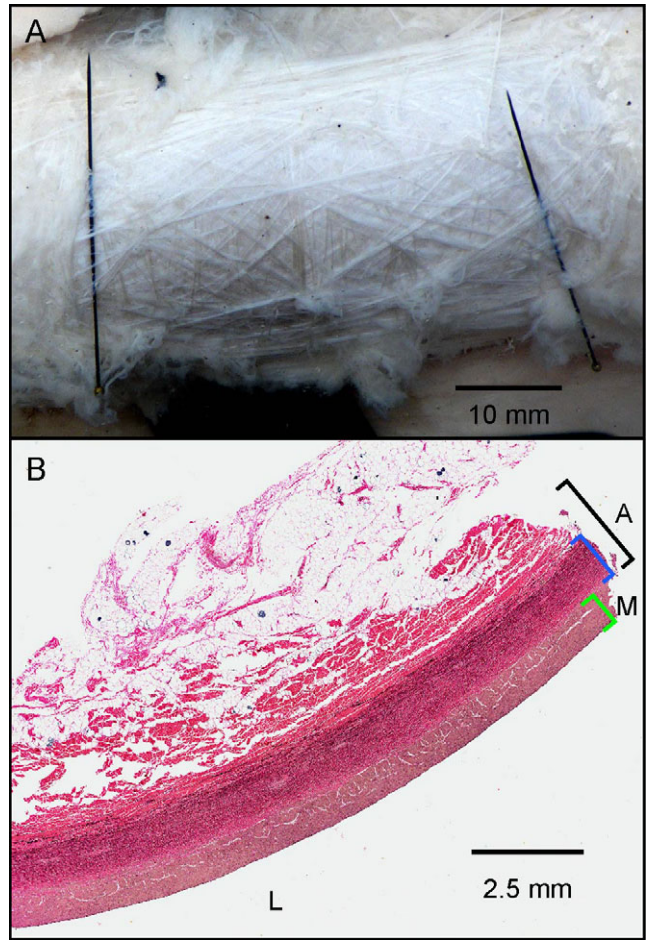

Fig. 1. Macroscopic morphology of fin whale internal thoracic artery. (A) Taut collagen fibres on the outside of an artery pressurized to 21 kPa (158 mmHg). Pins were used to measure longitudinal stretch. (B) Histological section cut longitudinally showing relative thickness of the layers. L, lumen; M, media; A, adventitia. The green bracket shows the full media, the black bracket shows the full adventitia and the blue bracket shows the portion of adventitia that contains lamellar elastin. Total wall thickness 4.33 mm: media, 0.78 mm; adventitia with lamellar elastin, 1.5 mm; adventitia with collagen but no lamallar elastin, 2.05 mm. Elastic Van Gieson stain. The curvature along the lumenal side is presumably due to elastin tissue retraction and would not exist *in vivo*.

Retial tissue was collected from the thoracic rete within the thorax and its cervical extension into the neck, deep to the scalene muscle, and from the basicranial rete, derived from the facial artery, from the cavity between the tympanic bulla and the mandible articulation (Ommanney, 1932). The thoracic rete consisted largely of arteries, ranging in size from 1 to 5 mm OD, with a few veins. Most arteries were embedded in adipose tissue, although some were embedded in collagen. About 15% of the rete cross-sectional area was occupied by arterial lumen, slightly lower than the 22% reported for narwhal,

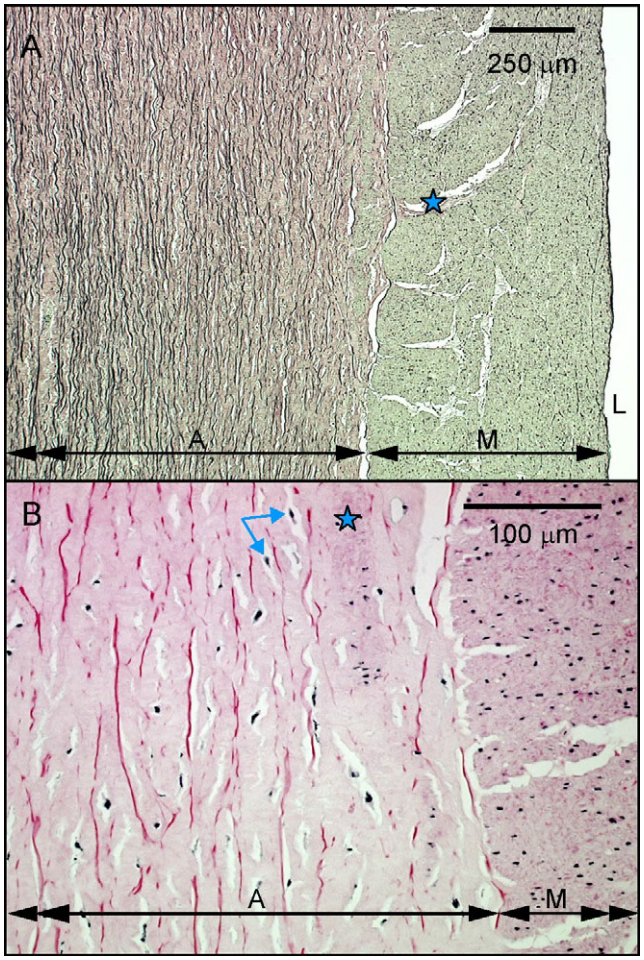

Fig. 2. Histology of fin whale internal thoracic artery cut longitudinally. (A) Low magnification showing intima (thin, dark edge along lumen, L), through media (M) to part of adventitia (A). Elastic Van Gieson stain. Media contains muscle (green with black nuclei), collagen (pink) and mostly non-lamellar elastin (dark) with occasional elastin fibre. Muscle cell nuclei are cut in cross-section indicating that cells run circumferentially. Collagen is abundant, especially at fracture planes (star). Adventitia shows lamellar or fibrous elastin and collagen. (B) Higher magnification at transition between media and adventitia showing cell types. Hematoxylin and eosin stain. Muscle cells in media stain dark pink with black nuclei. Cells in adventitia are predominantly fibroblasts (blue arrows), although there is a vertical band of smooth muscle cells (star). Red-staining elastin fibres run both parallel and perpendicular to the cut face. Collagen stains light pink.

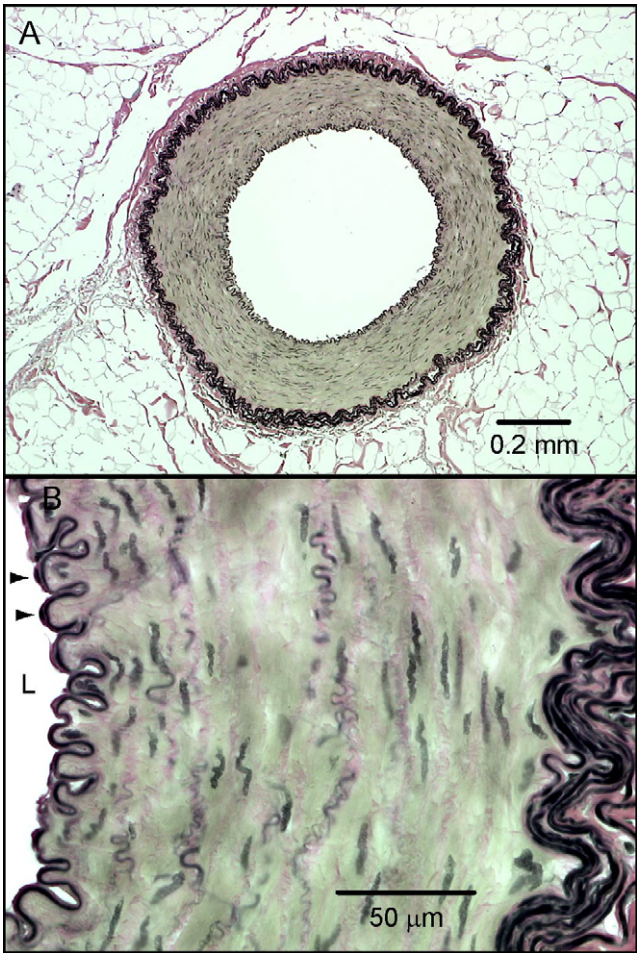

Fig. 3. Cross-section of artery from fin whale thoracic rete. (A) Muscular wall with internal elastic lamina (dark) and several external elastic lamellae interlaced with collagen. Some arteries were embedded in adipose, as shown, and others in collagen. (B) Higher magnification showing circumferential smooth muscle nuclei (dark), wavy elastin (dark) and wavy collagen (pink). Endothelial cells are visible in the intima (arrowheads). Elastic Van Gieson stain. L, lumen.

Monodon monoceros, and beluga, *Delphinapterus leucas*, by Vogl and Fisher (Vogl and Fisher, 1982). The arteries were muscular (Fig. 3), showing an internal elastic lamina, a thick media consisting of vascular smooth muscle, non-lamellar elastin fibres and collagen fibres, and an adventitia consisting of lamellar elastin and collagen. The basicranial rete showed histological structure similar to that of thoracic rete and rete of other cetaceans (Mcfarland et al., 1979; Pfeiffer and Kinkead, 1990; Vogl and Fisher, 1982; Walmsley, 1938).

Artery inflation tests

Individual arteries used in inflation tests were selected to cover a wide range of locations along the arterial tree. Fig. 4 shows the average passive response of nine non-retial arteries, the average response of six retial arteries, and the individual responses of the proximal and distal subclavian artery and, in Fig. 4B, the external carotid artery. The mean response of the pig thoracic aorta is shown for comparison as representative of terrestrial artiodactyla. With the exception of the subclavian artery, all arteries, both retial and non-retial, were very stiff circumferentially. They exhibited minimal compliance at low pressures, attaining a circumferential stretch λ_θ of only 1.10 by 5 kPa, which indicates collagen recruitment at very low pressures. Circumferential stretch increased minimally with higher pressures. By contrast, the subclavian artery was unusually compliant at low pressures, stretching readily to over 1.5 before it stiffened abruptly at 3 kPa. This artery ruptured at 8 kPa due to a gash from a flensing knife. Our observed responses are in accord with those reported by Shadwick and Gosline (Shadwick and Gosline, 1994): the high circumferential compliance of the left subclavian is similar to that reported for the aortic arch, brachiocephalic (innominate) and right common carotid, with the exception that the carotid stiffened at ~15 kPa and the arch at ~22 kPa, while the high circumferential stiffness of the external carotid and all other vessels is similar to that of the thoracic and abdominal aortas. The transition from compliant to incompliant occurred within the first branches off the aortic arch, with no further

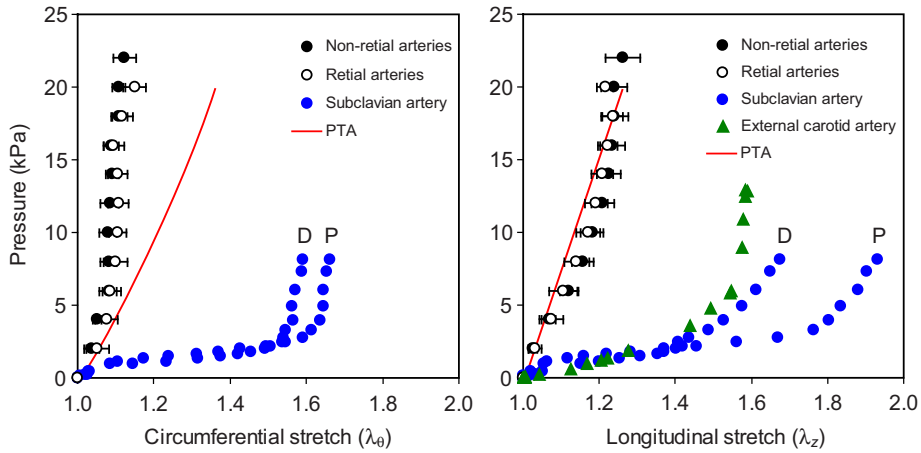

Fig. 4. Circumferential (left) and longitudinal (right) responses of fin whale arteries to untethered inflation. Solid symbols with error bars show means ± s.e.m. of nine non-retial arteries (eight for right panel). Solid symbols without error bars show individual responses of proximal (P) and distal (D) sections of a subclavian artery. Open circles with error bars show means ± s.e.m. response of six retial arteries. Triangles show the longitudinal response of an external carotid. Lines show the mean response of the pig thoracic aorta (PTA). Standard errors for the pig arteries are not shown, but are the same or smaller than those for the whale arteries. Left: the response of the subclavian artery differed from all others tested, stretching readily up to 3 kPa and then stiffening at higher pressures. All other arteries stretched minimally at low pressures and then stiffened. No artery showed the progressive stiffening typical of terrestrial mammals. Right: all arteries stretched more longitudinally than circumferentially, most to the same extent as the pig aorta. The subclavian artery and external carotid were more compliant than the others.

changes along the arterial tree (Fig. 5). No arteries showed the progressive stiffening typical of terrestrial mammals with a graded response over the physiological range. This relative independence of fin whale artery diameter to transmural pressure is consistent with our hypothesis that the arteries are subjected to widely varying transmural pressures *in vivo*.

In all arteries the longitudinal stretch response was greater than the circumferential (Fig. 5), and when the subclavian and external carotid arteries are excluded, the longitudinal stretch was about the same as that observed in the pig aorta (Fig. 4). Vessels in this study were tested untethered, which allowed observation of the longitudinal pressure response; however, these arteries are tethered *in vivo*, except for the subclavian artery and the retial arteries. Tissue harvesting was at times opportunistic and *in situ* longitudinal stretch could not be determined for all samples, but where measured, longitudinal stretches were typically around λ_z=1.4. Inflating the arteries without *in vivo* longitudinal tethering limits the information we can derive from these tests, but it has no impact on the ability of recruited collagen to restrict circumferential stretch (Lillie et al., 2012), which is our main focus. Abundant collagen was visible on all the arteries and could be readily removed from the retial arteries. This process increased the stretch at 13 kPa by 30% in the circumferential direction, making it similar to the stretch observed in the pig aorta, and by 12% in the longitudinal direction (Fig. 6). Thus the predominant functional orientation of the retial collagen was circumferential.

It has been hypothesized that the thoracic rete act as capacitance vessels, filling with blood during a dive as air volume diminishes. We tested this hypothesis by determining their capacitance, including longitudinal expansion because they are untethered *in vivo*. To compare arteries of different size, the volume for each artery at any pressure was normalized by the average volume for that vessel between 7 and 20 kPa. The results from seven thoracic rete and, for comparison, from three basicranial rete are shown in Fig. 7. For a pressure increment from 9 to 18 kPa the thoracic rete increased in volume by 14%. This is a small response, no larger than that of the basicranial rete, which lie outside of the thorax and presumably cannot participate in air volume replacement. By comparison, the same pressure shift would have increased the volume of the aortic arch by 79% (Shadwick and Gosline, 1994).

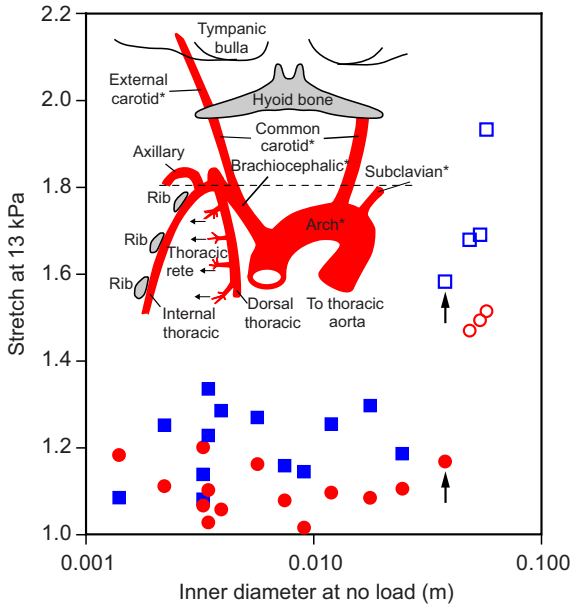

Fig. 5. Impact of position along the fin whale arterial tree on arterial mechanics, using diameter as a proxy for position. In all arteries, longitudinal stretch (squares) was greater than circumferential (circles). Only the largest arteries (open symbols), closest to the heart, showed significant compliance. All other arteries showed the same, minimal compliance. Subclavian artery stretch (right-most points) was measured at three axial positions and became progressively stiffer with distance from the heart. The external carotid (arrows) stretched longitudinally like the subclavian but circumferentially like the smaller vessels. Inset shows the major arterial branches of the aortic arch, redrawn from Walmsley (Walmsley, 1938). The broken line shows the anterior limit of the pleural domes (Ommanney, 1932). Asterisks show arteries with large compliance from the present study or Shadwick and Gosline (Shadwick and Gosline, 1994).

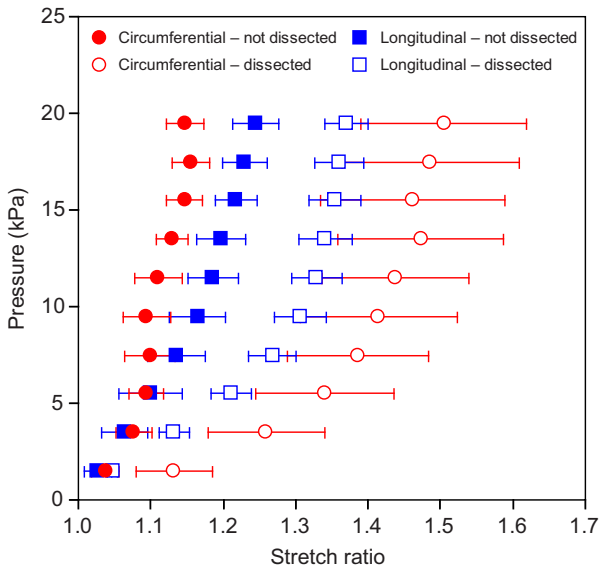

Fig. 6. Impact of adventitial collagen on average pressure stretch response (mean ± s.e.m.) of fin whale retial arteries. Removal of the adventitia (dissected) increased the circumferential stretch at 13 kPa by 30% and the longitudinal stretch by 12%. The predominant functional orientation of the adventitial collagen was circumferential.

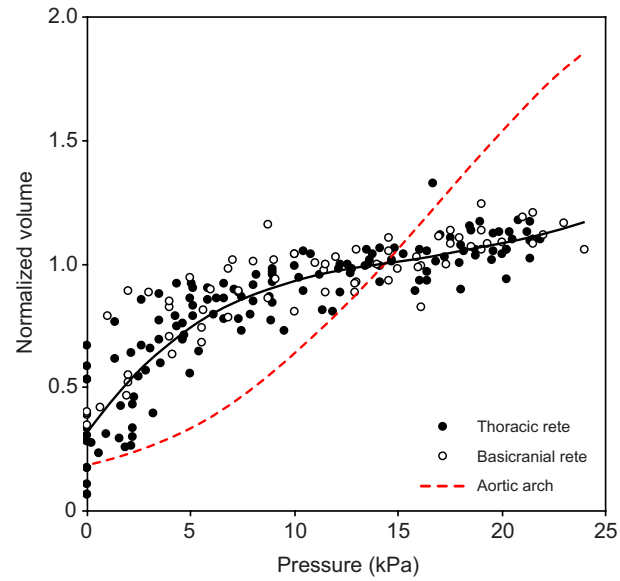

Fig. 7. Total capacitance of fin whale thoracic retial arteries (N=7) and basicranial rete (N=3). The volume for each artery has been normalized by the average volume for that vessel. The solid line is fit to the thoracic rete. The broken line shows comparable normalized volume of the aortic arch using data from Shadwick and Gosline (Shadwick and Gosline, 1994). Between pressures of 9 and 18 kPa the thoracic rete increased in total volume by ~14%. Capacitance of the thoracic rete was not greater than for the basicranial rete. Over the same pressure range the arch increased in volume by 79%. Total physiological volume for the thoracic rete is between 25 and 100 l and for the arch is 56 l.

Artery uniaxial tests

The circumferential secant moduli of two whale arteries subjected to uniaxial extension are shown in Fig. 8. A maxillary artery branch represents the behaviour of the stiff arteries and the subclavian artery represents the behaviour of the highly compliant arteries. Both have a non-linear response but the subclavian stretched considerably before collagen recruitment started, while the maxillary was stiff after little or no extension. For comparison, the modulus-stretch response of the thoracic aorta of a pig is shown by the solid line.

Artery collapse tests

The impact of negative transmural pressure on the collapse of individual arteries is shown in Fig. 9. Buckling generally occurred towards the flow outlet, and in most cases self-excited oscillations were present, behaviours typically exhibited by collapsible tubes (Bertram, 1987; Conrad, 1969). Collapse was associated with a reduction in flow, but flow did not stop. The protocol was to approach P_{collapse} from the collapsed (low flow) state, but substantial hysteresis in the flow response made it difficult to establish a precise point in some cases, particularly in the smallest vessels, in which flow volume was low even at full flow. This and the fact that many of the arteries were not circumferentially uniform introduced scatter into the response, but nonetheless we obtained a strong correlation showing that arteries with relatively thinner walls were less able to withstand negative pressures. Such a relationship is expected from the theory of tube stability (Bertram, 1987; Fung, 1984), and the data were plotted as a function of H^3/R^3 to use the theory to identify the factors affecting collapse.

The point at which a thick-walled tube collapses when exposed to negative transmural pressure depends on its bending rigidity, D:

$$D = \frac{E_\theta H^3}{12(1-\nu^2)}, \tag{7}$$

where E_θ is the elastic modulus, H is the undeformed wall thickness and ν is Poisson's ratio. The most likely mode of collapse of a circular vessel is into an ellipse and then a figure-of-eight, and for that mode, buckling is predicted to occur when the pressure exceeds $3D/R^3$:

$$P_{\text{collapse}} = \frac{3E_\theta H^3}{12(1-\nu^2)R^3}, \tag{8}$$

where R is the logarithmic mean radius:

$$R = \frac{R_o - R_i}{\ln(R_o / R_i)}. \tag{9}$$

If Eqn 8 applied to the behaviour of arteries we should see a linear relationship between P_{collapse} and H^3/R^3 in Fig. 9, which is not the case. Eqn 8 assumes Hookean elasticity, but the arterial mechanical response shown in Fig. 8 is decidedly non-linear, and this likely accounts for much of the non-linearity of the P_{collapse}–H^3/R^3 response. The stretch in a bending beam is compressive on one side and tensile on the other, remaining at zero at its neutral axis. Stretch increases linearly with distance from the neutral axis, making peak stretches greater in thicker beams. Therefore, the arteries represented by data points at the right of Fig. 9 will have been subjected to larger strains and hence, from Fig. 8, will have exhibited a higher modulus. Eqn 8 should therefore predict the response more closely if a stretch-dependent modulus rather than a constant modulus were used. To calculate the stretch of the collapsing artery wall we made the following assumptions: (1) geometry was circular in the unloaded vessel and elliptical at the collapse point, (2) the perimeter of the artery at the neutral axis was constant, (3) the position of the neutral axis from the inner wall was 30% of the wall thickness (Yu et al., 1993), (4) shear strains were negligible (Yu et al., 1993), and (5) the resistance to deformation came from the stretch of the tissue at

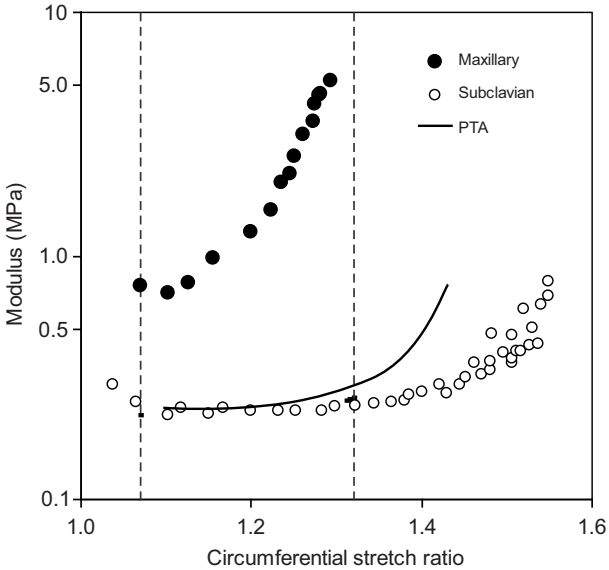

Fig. 8. Non-linear response of arterial rings stretched uniaxially in the circumferential direction. The maxillary artery branch represents the behaviour of the stiff whale arteries shown in Fig. 4 and the subclavian the behaviour of the compliant whale arteries. Solid line shows the response of the pig thoracic aorta (PTA). Stiffening due to collagen recruitment started at low stretches in the maxillary artery and at higher stretches in the subclavian and pig aorta. Moduli from the whale maxillary and from the pig aorta were used in Eqn 8 to predict collapse pressure in arteries exposed to negative transmural pressures, shown in Fig. 9. The vertical lines show the stretch range of the collagen-rich adventitia calculated for the collapsed arteries in Fig. 9 (see Results).

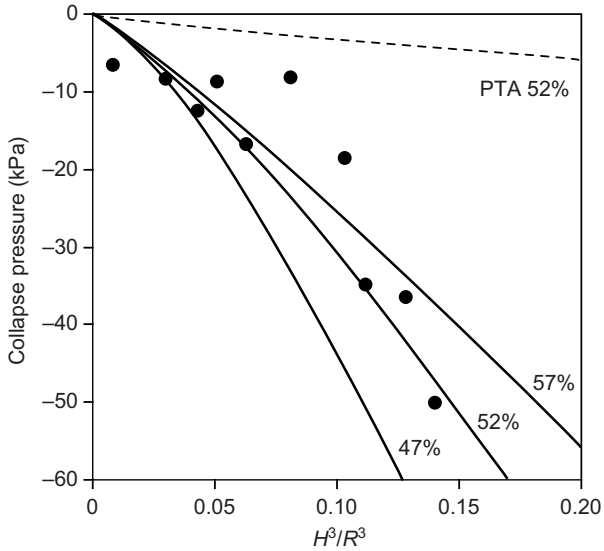

Fig. 9. Impact of morphology and modulus on negative transmural pressure at which fin whale arteries collapsed. Morphology was quantified by the ratio of wall thickness H to the logarithmic mean radius R measured in the unloaded artery. Collapse pressure was the point at which flow limitation ceased as negative pressure was reduced towards zero. Arteries with relatively thinner walls collapsed at pressures around –10 kPa while those with relatively thicker walls could withstand pressures of –50 kPa. The three solid lines show the collapse pressure predicted with Eqn 8 using the non-linear modulus-stretch properties of the maxillary artery shown in Fig. 8. The cross-sectional area of the lumen was reduced to 57, 52 or 47% of the undeformed value. The broken line shows the predicted collapse pressure for a pig thoracic aorta (PTA), with area reduced to 52%, based on the pig aorta modulus shown in Fig. 8. Arteries tested: internal thoracic, right coronary, dorsal thoracic, terminal branches of external carotid in ventral groove blubber (2 samples), intercostal, basicranial rete (3 samples) and posterior intercostal.

the smallest radius of curvature. In our experiments we gauged the point of collapse from flow limitation and did not measure the actual decrease in luminal cross-sectional area, but collapse generally occurs at an areal reduction to 50% of the unloaded area (Fung, 1984). We therefore determined stretches for a range of area ratios as well as a range of H/R. Stretches of the inner, middle and outer portions of the wall were calculated and translated into a weighted average modulus using modulus-stretch data from the maxillary artery shown in Fig. 8, assuming the modulus of the tissue was the same in compression and tension. The error associated with this assumption is likely a 0 to 3 kPa overestimation of $P_{collapse}$ for the whale tissue and less than 1 kPa for the pig tissue, based on the relationship between tensile and compressive moduli for the pig aorta at the relevant strains (Lillie et al., 2010). The predicted responses using Eqn 8 and the stretch-dependent modulus with a value of 0.29 for Poisson's ratio (Cox, 1978; Lillie et al., 2010; Patel et al., 1969) are shown by the three solid lines in Fig. 9. The curve that best approximated the experimental data was based on an area ratio of 52% at the collapse point. It fit the data better than a linear model although the curvature still appears underestimated. However, we applied the modulus-stretch response of the maxillary artery to all arteries, and it is possible that the mechanics, Poisson's ratio, or location of the neutral axis varies with vessel size. The other two curves show the predicted pressures required to reduce the area ratio to 57% and 47%. To reduce the luminal area of an artery with H^3/R^3=0.07 (H/R_1=0.50) to 57% would take a pressure of −16 kPa; to reduce it to 52% would take −19 kPa, and to reduce it to 47% would require −25 kPa. Thus the ever-increasing stiffness of the wall should make it progressively more difficult to collapse an artery, and this would inhibit flow restriction. The key factor in determining the response is the stretch of the collagen-rich adventitia: to reduce the area to 52%, the outer wall of the arteries at the left of Fig. 9 with the relatively thin walls stretched 7% and the thicker walled arteries at the right stretched 36%. These stretches are indicated by the vertical lines in Fig. 8. At 7% stretch the maxillary artery was already stiffened by collagen recruitment, but by contrast the subclavian and pig thoracic aorta had not stiffened even at 36% stretch, which means their adventitial collagen would not resist bending. Applying the same analysis to the pig aorta using measured pig aorta mechanics yielded the dotted line in Fig. 9, predicting collapse under relatively small pressures. Thus the early recruitment of collagen in the majority of whale arteries may represent an adaptation that inhibits their collapse under negative pressure.

The data in Fig. 9 indicate that some arteries would readily collapse under a negative transmural pressure while some would not, depending on H/R. To better understand the biological impact of this we have plotted H/R for all whale arteries studied (Fig. 10), including selected rat arteries for comparison. Values are plotted as a function of inner radius, using a log-log plot to cover the wide range of values. For both animals there is a trend towards relatively thicker walls in the smaller vessels, in part reflecting the transition from elastic to muscular arteries with distance from the heart. Eqn 8 identifies wall thickening as a potential adaptation to delay collapse, but there is no evidence in Fig. 10 that this has occurred: compared with the rat, the walls of the whale arteries are not overly thick given their radius. Nor does there appear to be any difference

between thoracic and extrathoracic arteries, although a difference would be expected if transmural pressures were constant around 13 kPa within the thorax but varied in the extrathoracic tissues.

We have used the relationship defined by the 52% curve of Fig. 9 to predict the collapse pressures for whale arteries based on their morphology, with the predicted values shown on the right ordinate of Fig. 10. To predict the response of the smallest vessels we have extrapolated far beyond our experimental range (−50 kPa), and it is quite possible that E_θ and ν vary with size, so their predicted pressures are only suggestive. The medium and smaller whale arteries appear to be protected from collapse by their relatively thick walls. Assuming the greatest negative pressure likely encountered *in vivo* is −30 kPa, then any artery with an inner radius smaller than ~0.004 m (OD 0.011 m; e.g. maxillary) would not collapse. Larger arteries are predicted to collapse, and the largest appear capable of withstanding only a small negative transmural pressure. However, most of these larger arteries are in the thorax, which would protect them from collapse. A small group of extravascular arteries lies between these protected extremes and are predicted to collapse should negative pressures of −5 to −30 kPa be generated during a dive.

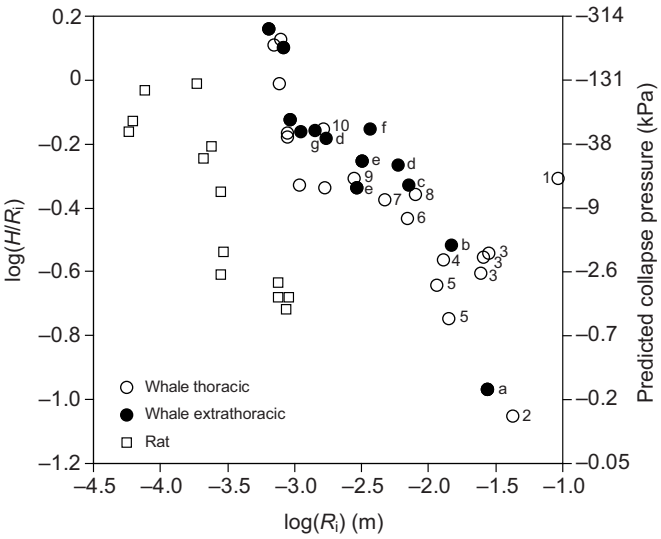

Fig. 10. Relative wall thickness of fin whale arteries, expressed as H/R_i, and predicted collapse pressure. Rat arteries are included for comparison. In both whale and rat, smaller arteries tended to have relatively thicker walls. Whale arteries did not have proportionately thicker walls than rat, which is contrary to the prediction from Eqn 8. There were no apparent differences between whale arteries from inside or outside the thorax. Right ordinate gives the collapse pressure predicted from Eqn 8 using the 52% line in Fig. 9. Smaller vessels appear protected from collapse by their thick walls, and most of the largest vessels, predicted to withstand only small pressures, are protected within the thorax. Only extrathoracic arteries with inner radii from 0.01 m (e.g. external carotid, –6 kPa) to 0.004 m (maxillary branch, –30 kPa) are predicted to be vulnerable to collapse. Whale thoracic arteries: 1, aortic arch; 2, thoracic aorta; 3, left subclavian; 4, common carotid; 5, internal thoracic; 6, dorsal thoracic; 7, intercostal; 8, right coronary; 9, posterior intercostal; 10, right coronary branch; not labelled, thoracic rete. Whale extrathoracic arteries: a, abdominal aorta; b, external carotid; c, maxillary; d, terminal branches of external carotid in ventral groove blubber; e, maxillary br; f, cervical plexus; g, alveolar; not labelled, cervical rete or basicranial rete. Whale arteries 1, 2 and a were taken from Shadwick and Gosline (Shadwick and Gosline, 1994). Rat arteries: thoracic aorta (proximal and distal), abdominal aorta (proximal and distal), carotid, iliac (common, external, internal), femoral, femoral branch, mesentary, intestinal and cerebral.

Resistance to collapse is vital to control flow through vascular beds during a dive. The standard diving response demonstrated in forced submersions (in the absence of exercise) includes peripheral vasoconstriction (Bron et al., 1966; Irving et al., 1942; Murdaugh et al., 1968; Zapol et al., 1979). However, the response in voluntary dives appears to be more flexible (Kooyman et al., 1981), with flow remaining in some vascular beds such as the adrenals in Weddell seals (Zapol et al., 1979), in the muscle beds of harbour (Jobsis et al., 2001) and Weddell seals (Guppy et al., 1986; Ponganis et al., 1993), and in the epaxial muscles of bottlenose dolphins *Tursiops truncatus* (Ridgway and Howard, 1979). It would not be possible to actively and selectively redistribute blood flow to different vascular beds if flow shut down passively under pressure.

DISCUSSION

The mechanical properties of mammalian arteries reflect the loads they experience *in vivo*. The inflation tests in this study showed that, except for a few branches just off the aortic arch, all arteries in a fin whale became unusually stiff at low transmural pressures compared with the terrestrial standard (Figs 4, 5). Similar behaviour was reported for the fin whale descending aorta (Shadwick and Gosline, 1994), and the high stiffness may be an adaptation that benefits the whale during a dive. The most prominent arterial adaptation in a diving mammal is the expansion of the aortic arch that allows it to function as a Windkessel, and a high aortic stiffness could facilitate this function by creating a strong reflection point to terminate the arch (Shadwick and Gosline, 1994). The classic Windkessel model requires instantaneous pressure transmission throughout the Windkessel chamber, allowing zero phase between pressure and volume. This requires a chamber of finite length relative to pressure pulse wavelength (Quick et al., 1998; Quick et al., 2006; Westerhof et al., 2009), and this is effectively produced in the fin whale by the major (92%) wave-reflecting junction between the arch and the descending aorta. Concentrating all compliance in the arch rather than distributing it through the aorta is predicted to minimize aortic impedance and peak systolic pressure (Campbell et al., 1981); it also eliminates any contribution to total arterial compliance and resistance from distal vascular beds whose properties change with depth, and it may prevent retrograde aortic flow at depth (Shadwick and Gosline, 1994).

All of these benefits could be realized by limiting arterial compliance over the physiological pressure range (generally taken as 10–16 kPa), yet the data in Fig. 4 show that collagen is recruited in most arteries at a few kPa of pressure, which allows very little compliance at any pressure. Further, the fin whale aortic arch maintains an essentially linear pressure–volume relationship up to 22 kPa (Shadwick and Gosline, 1994). These observations raise the question of whether diving whales experience a greater range of transmural pressures than terrestrial mammals. Maintaining a constant arterial diameter and constant mechanical properties over widely varying transmural pressures might stabilize downstream flow conditions. When faced with maintaining cerebral perfusion under hemodynamic conditions that vary actively and passively with depth (Zapol et al., 1979), and when the resistance to flow depends on tube radius raised to the fourth power (Hagen–Poiseuille equation), it may be beneficial in a diving animal to minimize the impact of varying transmural pressure on flow dynamics. For arteries under negative pressures, the recruitment of collagen at low strains reduces the likelihood of collapse (Fig. 9).

Thus understanding the arterial mechanics of a diving fin whale requires more precise information on transmural and thoracic pressures than is presently available. Brown and Butler (Brown and Butler, 2000) suggested that pressures in thoracic and extrathoracic

compartments may differ by ~3 kPa, but did not offer an analysis. Increasing thoracic pressure to ambient requires reducing the air volume in the thoracic cavity, but the degree to which this happens depends on the stiffness of the two parts of the thorax wall – the body wall and diaphragm. Cetacean body walls are stiff compared with those of pinnipeds (Leith, 1976; Moore et al., 2011), and van Nie argued they were too stiff to deform significantly at depth (van Nie, 1987), although this conflicts with evidence of inwards compression in odontocetes (Hui, 1975; Moore et al., 2011; Ridgway et al., 1969). Brown and Butler (Brown and Butler, 2000) proposed deformation of the diaphragm as the main mode of thorax cavity collapse, and Moore et al. (Moore et al., 2011) suggested that the longitudinal orientation of the cetacean diaphragm could facilitate compression of the thoracic contents by the abdominal viscera. The relative contributions of the body wall and diaphragm likely vary with depth, and at greater depths, where air-filled spaces are highly compressed, small discrepancies between actual and ideal air volumes can generate significant pressure gradients. We therefore developed a mathematical model to estimate the volume and pressure changes in the thorax of a diving fin whale.

Model of diving thoracic pressures, P_{thor}

We modelled the static diving response of the thorax of an 18 m fin whale, selecting 18 m to allow direct use of published anatomical measurements (Lockyer and Waters, 1986) and inflation data of the aortic arch (Shadwick and Gosline, 1994). Morphological details were taken from the literature and from images obtained at necropsy of a 9 m fin whale collected by the Marine Mammal Stranding Program at the University of North Carolina, Wilmington (permitted by the NOAA SER Stranding Agreement) (Fig. 11A, Table 1). We assumed the lungs in Fig. 11A were at minimum air volume (MAV), which we took as 5% of total lung capacity (TLC) (Leith and Lowe, 1972; Scholander, 1940). Linear dimensions were adjusted to the size of an 18 m fin whale assuming isometric scaling. The model morphology is illustrated in Fig. 11B.

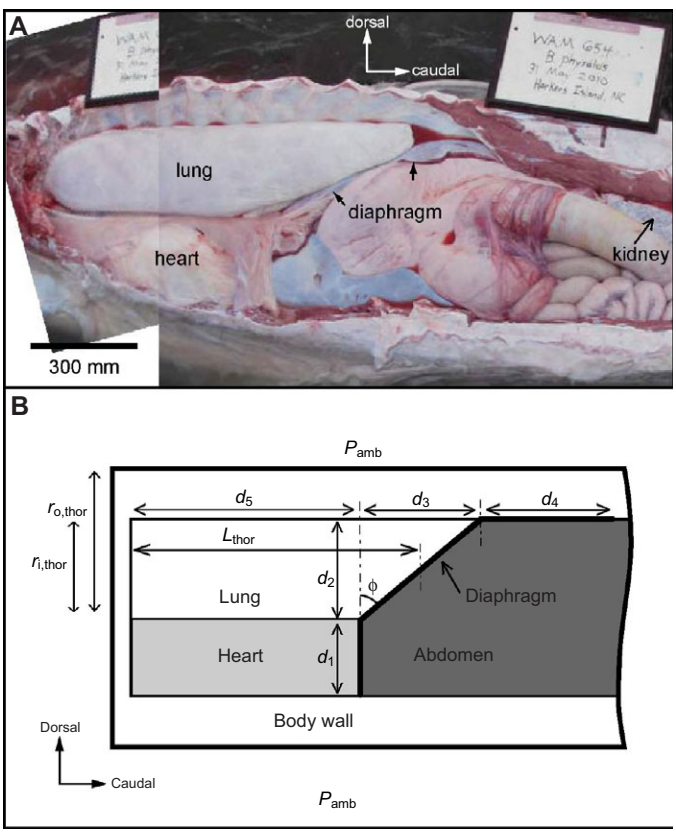

Fig. 11. Morphology used in modelling the diving response of the thorax of an 18 m fin whale. (A) Composite image of a 9 m female fin whale, WAM 654, obtained at necropsy (photo credit: W. A. McLellan). The whale was in shallow water, which minimized tissue distortion due to gravity. Ribs and diaphragm have been cut to expose left lung and abdominal viscera. Lung volume assumed to be at minimum air volume (MAV). Values for parameters at MAV are given in Table 1. (B) Simplified geometry showing parameters used to model the thorax. Geometry is for whale at total lung capacity near surface.

The ambient pressure, P_{amb}, at the surface was set at 101 kPa (1 atm) and increased by 101 kPa per 10 m depth. The pressure in the thorax, P_{thor}, was assumed uniform throughout. At the surface P_{thor} was taken as ambient pressure and at depth was calculated from Boyle's Law:

$$P_{thor}^{D} = \frac{P_{thor}^{S} V_{air}^{S}}{V_{air}^{D}}, \quad (10)$$

where the superscripts D and S indicate depth and surface, respectively, and V_{air} is the volume of air in the lungs. Air mass was assumed to be constant, prohibiting any gas exchange or exhalation part way through the dive. We assumed that fin whales dive on inspiration (Scholander, 1940), so V_{air} at the surface was set at TLC. V_{air} at depth was determined from the reduction in the total thorax volume, V_{thor}, as follows. The volume of the thorax was calculated as:

$$V_{thor} = \pi r_{i,thor}^{2} L_{thor}, \quad (11)$$

where $r_{i,thor}$ is the inner radius of the thorax and L_{thor} is the length of the thorax, shown in Fig. 11B. The thorax volume was the sum of V_{air} and tissue volume, V_{tissue}, the latter being largely composed of the heart, blood vessels, blood and lung parenchyma:

$$V_{thor} = V_{air} + V_{tissue}. \quad (12)$$

Tissue volume was calculated at MAV and was considered to be either constant during a dive or allowed to change by redistribution of blood. At the surface the air volume at TLC represented one-third (34%) of the total volume of the thorax. Inspiration to TLC at the surface increased $r_{i,thor}$ and L_{thor} from their values at MAV in Fig. 11A. We assumed L_{thor} increased as:

$$L_{thorTLC} = L_{thorMAV}\left(\frac{V_{thorTLC}}{V_{thorMAV}}\right)^{0.33}, \quad (13)$$

and used Eqn 11 to calculate the increase in $r_{i,thor}$. During a dive, V_{air} and V_{thor} decreased due to decreases in $r_{i,thor}$, determined by body wall compression, and L_{thor}, determined by diaphragm deformation.

Body wall compression

We modelled the body wall as a thick-walled, homogeneous, elastic cylinder with circular cross-section (Fig. 11B). The body wall encompassed the vertebrae, ribs and attached soft tissue, and the model predicted their average response. The model assumed zero longitudinal deformation (due to the vertebral column) and uniform circumferential deformation, although the observed response is non-uniform, greater on the ventral side (Moore et al., 2011; Ridgway et al., 1969). The body wall deformed according to the net force acting on it, F_{thor}, i.e. the difference between inward, F_{in}, and outward forces, F_{out}:

$$F_{thor} = F_{in} - F_{out}. \quad (14)$$

Table 1. Parameter values used to model the thoracic pressures in an 18 m diving fin whale

Structure	Value	Method	Source
Body length (L)	18 m		
Body mass (M)	33,000 kg	$0.0015L^{3.46}$	Lockyer and Waters, 1986
Total lung capacity (TLC)	1.440 m^3	$0.044M$	Leith and Lowe, 1972; Scholander, 1940
Diaphragm thickness, h_{diaph}	0.053 m	Isometric scaling	Dearolf, 2002
Heart dorsoventral thickness, d_1	0.670 m	Isometric scaling	WAM 654
Heart rostrocaudal length, d_5	1.85 m	Isometric scaling	WAM 654
Diaphragm rostrocaudal length, d_3+d_4	2.09 m	Isometric scaling	WAM 654
Length of diaphragm, L_{diaph}	3.06 m	Isometric scaling	WAM 654
Average length of thorax, L_{thor}	2.12 m	Isometric scaling	WAM 654
Outer thorax radius, $r_{o,thor}$	1.1 m	Isometric scaling	Lockyer and Waters, 1986; WAM 654
Inner thorax radius, $r_{i,thor}$	0.652 m	Isometric scaling	WAM 654

Values are given at minimal air volume (MAV), assumed to be 5% of TLC (two lungs). Dimensions taken from the image of a 9 m fin whale, WAM 654, shown in Fig. 11A, were scaled isometrically to an 18 m whale. Distances d_1 and d_3–d_5 are shown in Fig. 11B.

Inward, compressive forces arose from the outer ambient pressure acting over the outer thoracic surface area:

$$F_{in} = P_{amb} 2 r_{o,thor} L_{thor}, \quad (15)$$

and were resisted by the thoracic pressure acting over the inner thoracic area and by any mechanical forces developed in the tissue in response to deformation, F_{mech}:

$$F_{out} = P_{thor} 2 r_{i,thor} L_{thor} + F_{mech}, \quad (16)$$

where $r_{o,thor}$ is the external thoracic radius. If we consider only forces due to pressures, equilibrium would occur when:

$$P_{amb} r_{o,thor} = P_{thor} r_{i,thor}. \quad (17)$$

Because $r_{o,thor}$ exceeds $r_{i,thor}$, P_{thor} must therefore exceed P_{amb} at equilibrium. Whether this actually happens depends on the magnitude of the body wall mechanical forces: the stiffer the body wall, the more it resists deformation and the lower the required P_{thor} to offset compressive forces. For equilibrium, an excessively floppy body wall will require $P_{thor}>P_{amb}$, a very stiff body wall $P_{thor}<P_{amb}$, and only at a single, optimum body wall stiffness will $P_{thor}=P_{amb}$.

At equilibrium, the body wall mechanical force equals the mean circumferential stress on the body wall, $\langle\sigma_{thor}\rangle$, times the area of the tissue:

$$F_{mech} = \langle\sigma_{thor}\rangle 2\left(r_{o,thor} - r_{i,thor}\right) L_{thor}. \quad (18)$$

For a thick-walled cylinder, $\langle\sigma_{thor}\rangle$ is:

$$\langle\sigma_{thor}\rangle = \frac{P_{thor}\, r_{i,thor} - P_{amb}\, r_{o,thor}}{r_{o,thor} - r_{i,thor}}. \quad (19)$$

In the special case where $P_{thor}=P_{amb}$, Eqn 19 shows that $\langle\sigma_{thor}\rangle=-P_{amb}$. When $P_{thor}\neq P_{amb}$, stress is distributed non-uniformly across the wall. For a cylinder where the wall material is homogeneous, isotropic and obeys Hooke's Law, stress at any radial position $\sigma_{x,thor}$ is given by the Lamé equation (Humphrey and DeLange, 2004):

$$\sigma_{x,thor} = \frac{P_{thor} r_{i,thor}^2 - P_{amb}\, r_{o,thor}^2}{r_{o,thor}^2 - r_{i,thor}^2} - \frac{r_{i,thor}^2 r_{o,thor}^2 (P_{amb} - P_{thor})}{r_{o,thor}^2 - r_{i,thor}^2} \frac{1}{r_{x,thor}^2}. \quad (20)$$

We used Eqn 20 to determine that the radial position at which $\sigma_{x,thor}=\langle\sigma_{thor}\rangle$ was approximately one-third of the way through the wall from the luminal side, designated as $r_{1/3thor}$. Average stress correlates with the strain only at that point. The deformed thoracic radius at any wall position ($r_{x,thor}$) was calculated from $r_{i,thor}$ assuming constant wall volume:

$$r_{x,thor} = \sqrt{r_{i,thor}^2 - R_{i,thor}^2 + R_{x,thor}^2}. \quad (21)$$

Circumferential stretch ratios, λ^{thor}, were determined for any wall position as:

$$\lambda^{thor} = \frac{r_{x,thor}}{R_{x,thor}}. \quad (22)$$

The body wall secant modulus, E_{thor}, was calculated as:

$$E_{thor} = \frac{\langle\sigma_{thor}\rangle}{\varepsilon_{thor}}, \quad (23)$$

where ε_{thor} is the Green strain at $r_{1/3thor}$:

$$\varepsilon_{thor} = 0.5\left((\lambda_{1/3}^{thor})^2 - 1\right). \quad (24)$$

Diaphragm deformation

The diaphragm was modelled as attached to the ventral surface of the thorax immediately caudal to the heart, running vertically along the base of the heart to the lungs, then dorsocaudally along the lungs at an angle ϕ from the vertical to a variable point on the dorsal wall, and finally caudally in apposition to the body wall ending at the kidneys (Fig. 11). We considered two modes of diaphragm deformation: change in length and change in shape. A pressure gradient between the thorax and abdomen will stretch the diaphragm. When an elastic material is stretched or strained, strain energy is stored in the material and is available to power a recoil. Stretching the diaphragm elicits a resisting mechanical force in the diaphragm, and at equilibrium the force from the pressure gradient driving the diaphragm into the thorax balances the mechanical force pulling the diaphragm into the abdomen. Because a stretch can be maintained only in the presence of a driving force, stretching the diaphragm can reduce the pressure gradient, but it cannot wipe it out. The diaphragm can also change shape at constant length. A reduction of the thorax inner radius through body wall compression will create slack in the diaphragm, increasing the length of the apposition with the dorsal wall and possibly reducing the angle of the diaphragm, ϕ. Negligible strain energy is stored in the diaphragm on such deformation, so no pressure gradient is required to maintain the new position.

Diaphragm deformation was determined as follows, using a high stiffness to prevent strain or a low stiffness to allow strain. The abdomen was assumed to be at ambient pressure, creating a driving force for stretching the diaphragm determined by:

$$F_{diaph} = (P_{amb} - P_{thor}) \pi r_{i,thor}^2. \quad (25)$$

The resultant axial stress on the diaphragm, σ_{diaph}, was:

$$\sigma_{diaph} = \frac{F_{diaph}}{2\pi r_{i,thor} h_{diaph}}, \quad (26)$$

where h_{diaph} is the diaphragm thickness. We used a diaphragm thickness of 53 mm for the fin whale, based on isometric scaling of diaphragm thicknesses measured in bottlenose dolphins (Dearolf, 2002) and our unpublished measurements on a harbour porpoise and two Dall's porpoises, *Phocoenoides dalli*. The resultant strain of the diaphragm, ε_{diaph}, was:

$$\varepsilon_{diaph} = \frac{\sigma_{diaph}}{E_{diaph}}, \quad (27)$$

where E_{diaph} is the diaphragm secant modulus. The new diaphragm length, L_{diaph}, was calculated as:

$$L_{diaph} = L_{diaphTLC}(2\varepsilon_{diaph} + 1)^{0.5}. \quad (28)$$

From Fig. 11B and Pythagoras' theorem:

$$L_{diaph} = d_1 + (d_2^2 + d_3^2)^{0.5} + d_4, \quad (29)$$

where values for d_1 and the total distance d_3+d_4 are given in Table 1. d_2 was calculated as:

$$d_2 = 2r_{i,thor} - d_1. \quad (30)$$

Eqns 29 and 30 were solved for d_3. Finally, L_{thor} and ϕ were calculated as:

$$L_{thor} = d_5 + 0.5d_3, \quad (31)$$

$$\phi = \arctan(d_3/d_2). \quad (32)$$

Values for d_5 are given in Table 1.

We know of no studies on the mechanics of the cetacean diaphragm. The terrestrial mammalian diaphragm is composed of muscle, a collagenous central tendon and an elastin-rich ligament (Griffiths et al., 1992), each with different mechanical properties. Diaphragm muscle moduli range from 0.2 to 0.8 MPa (Coirault et al., 1998; Gates et al., 1980), and a value of 33 MPa has been used to model the tendon (Behr et al., 2006). The central tendon may be reduced or absent in cetaceans (Dearolf, 2002), but diaphragm movement may be constrained by other structures, including surface tendons that may be comparable to the elastic ligament and dorsolateral connective tissue connections to the subdermal sheath (Dearolf, 2002). We assumed that a modulus value of 15 MPa represented the average value of all tissue types.

Isolated fin whale lungs appear to collapse to their dead space volume (Scholander, 1940). Scholander measured the dead volume of the trachea, bronchi and bony nasal canals in a fin whale as 6.5% of TLC from which alveolar lung collapse in a fin whale diving at TLC is predicted to occur at 150 m. We assumed all volume collapse occurred in the alveoli and modelled the response down to 150 m. This does not take into account possible partial collapse of trachea and so the collapse depth may be underestimated (Bostrom et al., 2008; Fahlman et al., 2009; Kooyman et al., 1970).

We used the model to explore four scenarios. Case 1 determined the optimum stiffness of the body wall, $E_{thor,optimum}$, required to set P_{thor}=P_{amb}. The diaphragm changed shape but remained at constant length, with E_{diaph}=10^5 MPa. P_{thor} was calculated by iteratively applying Eqns 10–32, decrementing the value of E_{thor} from an initial value of 30 MPa until P_{thor} matched P_{amb}. Case 2 considered the consequence of a suboptimal body wall stiffness when the diaphragm changed shape but remained at constant length, with E_{thor}=1.02$E_{thor,optimum}$ and E_{diaph}=10^5 MPa. Case 3 is similar to Case 2, but with E_{diaph}=15 MPa to allow the diaphragm to strain. Case 4 is similar to Case 3, but with various volumes of blood shifted into the thorax.

Model predictions of thoracic pressure

The first run of the model (Case 1) assumed static equilibrium and no change in response to ambient pressure other than body wall compression and the associated passive rearrangement of the diaphragm at constant length. Using appropriate parameter values, the modelled thorax could be pressurized to ambient level, with P_{thor}=P_{amb}. To achieve this at a depth of 100 m (i.e. at 11 atm), outer diameter was reduced by 5% and inner diameter by 12%. These values agree with the 5 and 12% responses of a harbour porpoise at equivalent depth in a hyperbaric chamber measured using computed tomography (Moore et al., 2011) (from their fig. 2), and the 16% maximal inner diameter reduction in bottlenose dolphins and pygmy and dwarf sperm whales *Kogia breviceps* and *K. sima* (Piscitelli et al., 2010). At a depth of 100 m, the length of the modelled thorax decreased by 10% through movement of the diaphragm: the apposition between diaphragm and dorsal chest wall increased with depth, and the angle of the diaphragm became slightly more vertical (Fig. 12). This response is lower than the 30% length change observed in a harbour porpoise in a hyperbaric chamber (Moore et al., 2011) (from their fig. 3).

The values of E_{thor} required to achieve P_{thor}=P_{amb} and the associated stress–strain curve for the body wall are plotted as a function of depth in Fig. 13. The Case 1 analysis showed that maintaining a thoracic pressure at ambient requires that the body wall exhibit a non-linear stress–strain response that perfectly matched modulus with depth. Biological stress–strain curves are generally non-linear, and the one shown in Fig. 13 is not unusual, but exactly matching response to depth is likely not possible because the conditions at a given depth are not unique, in part because the tissue loading differs on the descent and ascent portions of the dive, and in part because the response of biological materials to loading inherently depends on time. Three factors are of particular interest:

(1) Inertia. The masses of the thoracic and abdominal walls and contained viscera need a finite time to respond to a force (pressure), which creates a lag between force and displacement. Our model is based on static equilibrium, but equilibrium is presumably unattainable with peak descent rates exceeding 5 m s^{-1} and resultant pressure changes surpassing 50 kPa s^{-1} (Goldbogen et al., 2006). The response of both the thoracic and the extrathoracic tissues will lag any change in ambient pressure, and because volume deformation of the extrathoracic tissue is negligible compared with the air-filled thorax, the lag in the thoracic response should be greater.

(2) Viscoelasticity. We modelled the body wall as an elastic structure, but biological tissue is viscoelastic, and we assume this applies to all whale tissues. By definition, a viscoelastic response is dependent on time and loading rate: the full response to a load is not immediate, but the tissue continues to strain or creep over time, usually with logarithmic decay. The resultant phase lag between loading and deformation leads to hysteresis in a loading/unloading cycle, and as a result a portion of the energy stored in the tissue during deformation is dissipated as heat and so is not available to power a recoil. Biological tissues are generally biphasic, a mixture of solid and fluid, and fluid flow in response to local gradients (poroelasticity) gradually alters the tissue properties by shifting stresses from the liquid to the solid. Thus we expect the viscoelasticity of the tissue will result in a different tissue response on descent (loading) than on ascent (unloading).

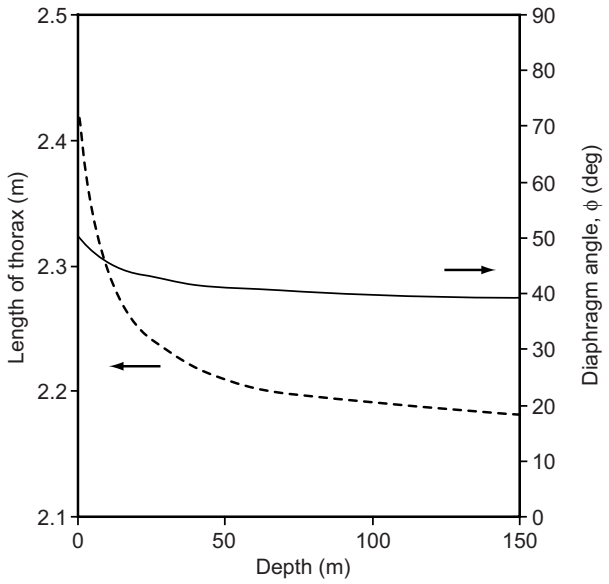

Fig. 12. Changes in thorax length and diaphragm angle predicted by the model to pressurize thorax to ambient level (Case 1). The model assumed static equilibrium and allowed only body wall compression and the associated passive rearrangement of the diaphragm at constant length. The thorax shortened and the diaphragm shifted slightly towards the vertical during the initial part of the dive and changed little in deeper water.

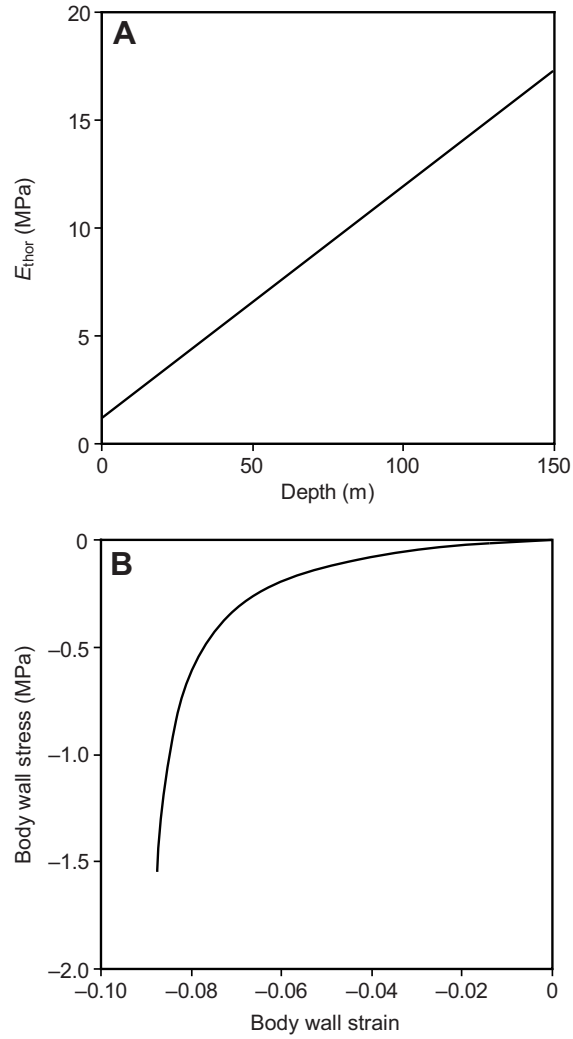

Fig. 13. Optimum body wall properties predicted by model to pressurize thorax to ambient levels (Case 1). The model assumed static equilibrium and allowed only body wall compression and the associated passive rearrangement of the diaphragm at constant length. (A) Body wall secant modulus at a depth of 0 to 150 m. (B) Body wall stress–strain properties.

(3) Swimming kinematics. Descent speeds for a fin whale average 3.7 m s^{-1} at an average pitch angle of −53 deg with respect to horizontal, and ascent speeds average 2.4 m s^{-1} at 64 deg (Goldbogen et al., 2006). The change in swim speed between descent and ascent will load the tissues at different rates (with inertial and viscoelastic consequences), and the change in body orientation will reverse the direction of any forces arising from differences in the specific gravity of the thoracic and abdominal viscera (Craig, 1963). Fin whales descend using a combination of glide and stroke-and-glide gaits and ascend with steady fluking (Goldbogen et al., 2006). Locomotor and respiratory muscles are mechanically coupled in terrestrial animals (Bramble, 1989; Young et al., 1992) and locomotor muscles may facilitate respiration in bottlenose dolphins (Cotten et al., 2008). Therefore, activation of the locomotor muscles during a breath-hold dive may alter thoracic pressures (Rommel et al., 2006), comparable to the Valsalva and Mueller manoeuvres in human divers (Balestra et al., 1998; Craig, 1963), with a potentially different impact on descent and ascent.

For the second run of the model (Case 2) we set E_{thor} 2% above optimum. Because the descent and ascent portions of a dive lack symmetry, thorax response cannot be optimized for both, and so the response must be suboptimal for at least for part of a dive. The impact of a suboptimal response on thoracic pressures can be quantified by altering tissue properties in the model, because the secant modulus incorporates any influence of time-dependent (inertia and hysteresis) and kinematic factors on the stress–strain relationship. The magnitude of hysteresis effects in the canine chest wall averaged 4% (Shardonofsky et al., 1990). The magnitude of inertial effects depends on descent rate and on any time delay between thoracic and extrathoracic tissue deformation. For a lag of 0.5 s at a descent rate of 3 m s^{-1}, depth increases 1.5 m during the lag time. The optimum modulus changes by 0.107 MPa per metre depth (Fig. 13), so the lagged modulus will be off by 0.16 MPa, representing an error of 2.5% at a depth of 50 m and 1.4% at 100 m. Based on these values, the model was allowed to reach equilibrium with E_{thor} set 2% above optimum.

The second run of the model predicted a thorax pressure below ambient, which was expected because we increased the body wall's ability to resist compression, and the difference between P_{thor} and P_{amb} increased with depth (Fig. 14A). (Had we set E_{thor} 2% below optimum, the responses would have been the same, but negative.) At 100 m the predicted difference was 14 kPa, about the maximum transdiaphragmatic pressure exertable in humans (Agostoni and Rahn, 1960; Laporta and Grassino, 1985), which would wipe out the transmural pressure in an extrathoracic artery. The discrepancy between the predicted air volume and the target volume required for P_{thor}=P_{amb} decreased with depth and was only 1.6 l at 100 m depth (Fig. 14B). Thus it appears that although a small mismatch in tissue properties has the potential to generate sizable pressure gradients, the associated volume discrepancies are small and might be removed by a small additional response by the diaphragm (Case 3) or a redistribution of blood volume (Case 4).

For the third run of the model (Case 3) we reduced the diaphragm modulus to 15 MPa to allow it to change length. It took minimal

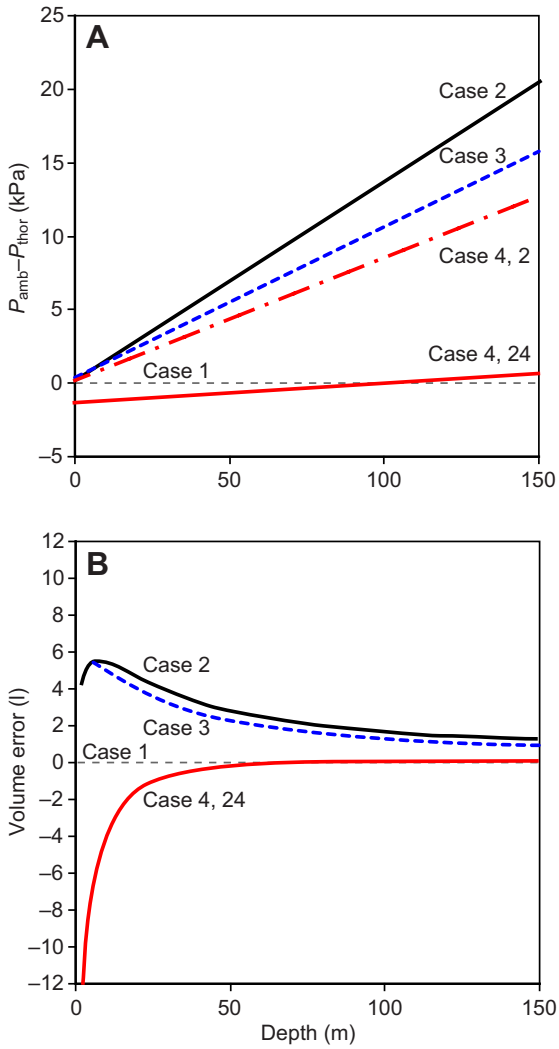

Fig. 14. Pressure gradients between thorax and ambient (A) and volume errors (B) predicted by the model when body wall stiffness was optimal (Case 1), when it was 2% higher than optimum to represent a lagged response without compensating blood redistribution (Cases 2 and 3) and a lagged response with compensating blood redistribution (Case 4). The model assumes static equilibrium. Volume error is the difference between the actual air volume predicted by the model and that calculated by Boyle's Law required to remove the pressure gradient. At optimal stiffness (Case 1) there are no pressure gradients or volume errors. At suboptimal stiffness pressure gradients increased with depth and volume errors generally decreased with depth. Significant pressure gradients developed when the diaphragm was allowed to deform but not strain (Case 2) and were smaller when diaphragm strain was permitted (Case 3). Allowing a fixed influx of 2 l of blood from the thorax (Case 4, 2) had minimal impact on the pressure gradient because the body wall and diaphragm readjusted to compensate. Allowing a fixed influx of 24 l (Case 4, 24) removed the pressure gradient at 100 m but created a small, opposite pressure gradient at shallower depths. Blood volume influx would have to be adjusted according to depth to remove all pressure gradients and volume errors.

diaphragm strain (<1%) to reduce the pressure gradients and the volume error (Fig. 14), suggesting larger pressure gradients could be accommodated, as long as diaphragm muscle strain remained within its physiological limits. However, as long as strain energy is stored in the diaphragm, the pressure gradient and the volume error cannot be reduced to zero.

For the final run of the model (Case 4) we allowed an influx of blood volume. Shifting small volumes (1–2 l) into the thorax had only a small impact on the thoracic pressure (Fig. 14A), because the body wall and diaphragm readjusted to compensate, but by shifting in 24 l, thoracic pressure at depths around 100 m could be raised to ambient. The volume required for pressure equilibrium varied with depth, requiring 24 l around 100 m, but only 11 l near the surface. Therefore, if shifting blood volumes offers a useful method of adjusting thoracic pressures, there needs be a reservoir of adequate volume that can rapidly adjust with depth, either passively or actively. Several vascular reservoirs in diving mammals have been identified for possible volume replacement: the aortic arch (Shadwick and Gosline, 1994), the thoracic rete (Barnett et al., 1958; Mcfarland et al., 1979; Walmsley, 1938), the tracheal rete (Cozzi et al., 2005) and venous structures within the thorax or associated with air-containing structures (Costidis and Rommel, 2012; Cozzi et al., 2005; Falke et al., 2008; Ninomiya et al., 2005).

Both the aortic arch and thoracic venous structures could change volume passively. Venous structures have received little attention in cetaceans (Costidis and Rommel, 2012), and there are currently insufficient data to determine the adequacy of their volume or compliance for regulation of thoracic pressure in a fin whale. The aortic arch for an 18 m fin whale has ample volume, holding ~56 l at 13 kPa and increasing essentially linearly with pressure from near zero to ~120 l at 22 kPa (Shadwick and Gosline, 1994). Passive arch compliance is ~10 l kPa^{-1}, so volume shifts of 11 to 24 l would require shifts in arch transmural pressure of 1.1 to 2.5 kPa. From either its peak systolic volume of ~75 l or end diastolic volume of ~40 l (Shadwick and Gosline, 1994), the arch could gain or lose 24 l without exceeding the linearity of its pressure–volume response, allowing bidirectional operation for both descent and ascent.

Passive influx requires a change in the vascular transmural pressures. Although arterial transmural pressures inside the thorax are reset at the systolic phase of a cardiac cycle, they change during diastole, in part according to normal blood outflow, but also due to any change in P_{thor}. At a normal heart rate, diastole lasts an estimated 3 to 6 s (Shadwick and Gosline, 1994), longer during dive bradycardia, and over this time P_{thor} and $P_{extrathor}$ could rise by 90 to 180 kPa. Unless the intra-arterial pressures rise with equal rapidity, transmural pressures will change. If changes in P_{thor} lag $P_{extrathor}$, as we assumed above, extrathoracic arteries would be squeezed first during descent. Their limited compliance would produce little movement of blood, and what 'retrograde' flow occurred (reduced forward flow) could be accommodated in the arch. The additional volume would raise intra-arterial pressure according to arch compliance, and transiently raise P_{thor}, according to thorax body wall compliance. Both responses would suppress further retrograde flow. Thus aortic arch and possibly thoracic venous structures could provide a passive, self-equilibrating mechanism that facilitates P_{thor} and $P_{extrathor}$ equalization, capitalizing on the low inertial lag of blood flow to provide a faster response than thoracic compression. Given enough time, blood redistribution could equalize compartmental pressures. However, the rate at which pressures equilibrate during diastole, if at all, cannot be determined with our present knowledge, and a pressure gradient will persist until equalization is attained. Therefore, each cardiac pulse may initiate a period of transient, diminishing pressure gradients that register as varying transmural pressures on all thoracic and extrathoracic arteries.

Active blood shifts through vasoactivity could improve response times, and, as is evident from Fig. 3, the thoracic rete are muscular arteries. The hypothesis that the thoracic rete provide a shiftable blood volume was dismissed by Scholander, who argued that the volume of the thoracic rete was much too small to be of significance (Scholander, 1940). We used the data from Fig. 7 to pursue this hypothesis. Based on the volume of thoracic rete measured in a

bottlenose dolphin relative to its lung volume and its body mass (Piscitelli, 2009), we estimated the total volume of fin whale thoracic retia to be 50 to 200 l, which is consistent with the 200 l estimated by Yablokov et al. (Yablokov et al., 1974). We found ~15% of this represented the blood within the lumen of the unpressurized arteries, corresponding to blood volumes of 8–30 l. The blood volume in the unpressurized thoracic rete represented ~30% of the total volume around physiological pressures (Fig. 7), so the total physiological blood volumes are likely 25 to 100 l. Because our model predicted that volume shifts of only 11–24 l are required to equalize pressure gradients, blood volumes in the thoracic rete appear adequate for them to modulate thoracic pressures, contrary to Scholander's view.

Direct neural control of retial arteries would allow rapid blood redistribution (Nagel et al., 1968), but although ample innervation runs in close proximity to dolphin and fin whale rete (Nagel et al., 1968; Ommanney, 1932), direct adrenergic connections have been shown to be poor in the rete of the narwhal (Vogl et al., 1981). Pfeiffer et al. (Pfeiffer and Kinkead, 1990), studying non-thoracic retial arteries from the bowhead whale, *Balaena mysticetus*, came to a similar conclusion based on a number of morphological features including the observation of ganglia-like complexes in the media, but no diffuse neurons. Cozzi and co-workers demonstrated the presence of nitric oxide synthase in peripheral neurons along venous lacunae in tracheal mucosa in the striped dolphin, *Stenella coeruleoalba*, and suggested local engorgement there occurs through nitric-oxide-mediated dilation (Cozzi et al., 2005). It is not know whether neuronal nitric oxide is involved in regulation of local flow through thoracic or other rete, nor the rapidity of the mechanism involved (Bohlen, 2011). If retial response time is slow, on the order of a minute, they may be able to coordinate blood flow with pressure changes on steady descents or ascents, which take 1–2 min (Goldbogen et al., 2006). It may prove difficult for the retial arteries to accommodate transmural transients generated by locomotor muscles during lunge feeding or strong fluking or transients associated with the cardiac cycle. However, if such transients were transmitted to the general arterial system, they would be without consequence because of the early collagen recruitment and unusual stiffness of the arterial walls (Fig. 4). As we have not considered spinal or cerebral arteries in this study, we cannot predict the impact of a transmural transient on cerebral vasculature. However, all cerebral flow passes through the thoracic rete (Walmsley, 1938). Whether pressure transients would be transmitted to the cerebral blood supply or filtered by the thoracic rete, as concluded by Nagel and co-workers (Nagel et al., 1968), remains to be examined.

Conclusions

Our model based on static equilibrium predicts that fin whales have the capacity to maintain a thoracic pressure close to ambient ocean pressure using a combination of non-linear body wall stiffness, diaphragm deformation and blood volume shift, but only if the responses maintain equilibrium. This prediction should be true as long as there is sufficient blood volume to be redistributed. However, equilibrium may not be reached quickly because of limited tissue response times, and equilibrium will not be reached at all while ambient pressures are changing during a dive. Therefore, a pressure gradient will exist across the thoracic wall for a significant portion of a whale's dive, including descent and ascent. The existence of transthoracic pressure gradients is unavoidable, but their impact on arterial transmural pressures can be controlled, and despite rapid descents, the model predicts that thoracic and arterial pressure gradients remain manageable in a diving fin whale. This prediction is necessarily based on assumptions about fin whale physiology and morphology, and closer examination of these assumptions is warranted to improve our understanding of the performance of whale's arterial system during diving.

Unlike terrestrial mammals, diving fin whales may lack precise control of arterial transmural pressures. The fin whale arterial system appears designed to be tolerant of pressure transients that could be unavoidable but also intentional. Minimizing the hemodynamic consequences of transients could widen the usable range of diving behaviours, such as stronger fluking or the deliberate use of respiratory muscles to alter thoracic volume. The primary aim of this study was to lay out what is known about the impact of thoracic pressures on arterial mechanics and what needs further examination. We believe that control of thoracic pressure is central to cetacean respiratory pathophysiology, dive and foraging energetics, and pathologies associated with decompression sickness. The questions raised in this study are important to arterial physiology but can be answered only through understanding the integration of all aspects of whale biology.

LIST OF SYMBOLS AND ABBREVIATIONS

d_1–d_5	thorax dimensions shown in Fig. 11B
E_{diaph}	modulus of diaphragm
E_{thor}	circumferential modulus of thorax
$E_{thor,optimum}$	circumferential modulus of thorax required to set $P_{thor}=P_{amb}$
E_θ	circumferential modulus of artery
F	circumferential load on artery in uniaxial tests
F_{diaph}	net force acting on diaphragm
F_{mech}	mechanical force of ribs resisting compression of thorax cavity
F_{thor}	net force acting on thorax
H, h	artery wall thickness in the unloaded and loaded artery
h_{diaph}	diaphragm thickness
ID	inner diameter
L, l	length of segment in the unloaded and pressurized artery
L_{diaph}	length of diaphragm
L_{thor}	length of thorax
MAV	minimum air volume
OD	outer diameter
P_{amb}	ambient ocean pressure
$P_{collapse}$	negative transmural pressure required to collapse artery
$P_{extrathor}$	extravascular pressure outside the thorax
P_{thor}	extravascular pressure inside the thorax
R	logarithmic mean radius of artery
$r_{1/3thor}$	thorax radius 1/3 of the way across the wall from the inside
$R_{1/3thor}$	unloaded thorax radius 1/3 of the way across the wall from the inside
r_i, r_{mid}, r_o	inner, midwall and outer radius of the pressurized artery
R_i, R_{mid}, R_o	inner, midwall and outer radius of the unloaded artery
$r_{i,thor}$, $r_{o,thor}$	inner and outer radius of thorax
$R_{i,thor}$, $R_{o,thor}$	inner and outer radius of the unloaded thorax
TLC	total lung capacity
V_{air}	volume of air in lungs
V_{thor}	total volume of thorax
V_{tissue}	volume of tissue in thorax excluding air
w	width of unloaded artery ring in uniaxial test
ε_{diaph}	diaphragm strain
ε_{thor}	circumferential strain on thorax
ε_θ	circumferential strain on artery
λ_j^{thor}	circumferential stretch of thorax where j represents r_o, r_{mid}, $r_{1/3}$ or r_i
λ_θ, λ_z	mean circumferential and axial stretches on artery
ν	Poisson's ratio
σ_{diaph}	stress on diaphragm
$\langle\sigma_{thor}\rangle$	circumferential stress on thorax
σ_θ	circumferential stress on artery
ϕ	diaphragm angle shown in Fig. 11B

ACKNOWLEDGEMENTS

The authors acknowledge the generous assistance provided by Kristian Loftsson of Hvalur and by the many workers at Hvalfjörður, Iceland. The authors would like to thank Jeremy Goldbogan and Nick Pyenson for their help in the field, Stephen Raverty for facilitating importation of the tissue, and Sam Gérard for the technical help in Vancouver. Special thanks to William McLellan at the University of North Carolina Wilmington Marine Mammal Stranding Program and to Vicky Thayer, Keith Rittmaster and all other volunteers who responded to the stranding event and provided the photos of WAM 654.

AUTHOR CONTRIBUTIONS

M.A.L., J.M.G. and R.E.S. were involved in the conception of the study and the design and execution of the mechanical tests. M.A.L., M.A.P. and A.W.V. were involved in the morphological studies. All authors were involved in the model development, interpretation of findings, and the writing of the manuscript.

COMPETING INTERESTS

No competing interests declared.

FUNDING

This work was supported by Discovery Grants from the Natural Sciences and Engineering Research Council to J.M.G. and to A.W.V., and by a Discovery Accelerator Grant from the Natural Sciences and Engineering Research Council to R.E.S.

REFERENCES

Agostoni, E. and Rahn, H. (1960). Abdominal and thoracic pressures at different lung volumes. *J. Appl. Physiol.* **15**, 1087-1092.

Armentano, R. L., Levenson, J., Barra, J. G., Fischer, E. I. C., Breitbart, G. J., Pichel, R. H. and Simon, A. (1991). Assessment of elastin and collagen contribution to aortic elasticity in conscious dogs. *Am. J. Physiol.* **260**, H1870-H1877.

Balestra, C., Germonpré, P. and Marroni, A. (1998). Intrathoracic pressure changes after Valsalva strain and other maneuvers: implications for divers with patent foramen ovale. *Undersea Hyperb. Med.* **25**, 171-174.

Bank, A. J., Wang, H. Y., Holte, J. E., Mullen, K., Shammas, R. and Kubo, S. H. (1996). Contribution of collagen, elastin, and smooth muscle to *in vivo* human brachial artery wall stress and elastic modulus. *Circulation* **94**, 3263-3270.

Barnett, C. H., Harrison, R. J. and Tomlinson, J. D. W. (1958). Variations in the venous systems of mammals. *Biol. Rev. Camb. Philos. Soc.* **33**, 442-487.

Behr, M., Thollon, L., Arnoux, P. J., Serre, T., Berdah, S. V., Baque, P. and Brunet, C. (2006). 3D reconstruction of the diaphragm for virtual traumatology. *Surg. Radiol. Anat.* **28**, 235-240.

Bertram, C. D. (1987). The effects of wall thickness, axial strain and end proximity on the pressure-area relation of collapsible tubes. *J. Biomech.* **20**, 863-876.

Bohlen, H. G. (2011). Rapid and slow nitric oxide responses during conducted vasodilation in the in vivo intestine and brain cortex microvasculatures. *Microcirculation* **18**, 623-634.

Bostrom, B. L., Fahlman, A. and Jones, D. R. (2008). Tracheal compression delays alveolar collapse during deep diving in marine mammals. *Respir. Physiol. Neurobiol.* **161**, 298-305.

Bramble, D. M. (1989). Axial-appendicular dynamics and the integration of breathing and gait in mammals. *Am. Zool.* **29**, 171-186.

Bron, K. M., Murdaugh, H. V., Jr, Millen, J. E., Lenthall, R., Raskin, P. and Robin, E. D. (1966). Arterial constrictor response in a diving mammal. *Science* **152**, 540-543.

Brown, R. E. and Butler, J. P. (2000). The absolute necessity of chest-wall collapse during diving in breath-hold diving mammals. *Aquat. Mamm.* **26**, 26-32.

Campbell, K. B., Rhode, E. A., Cox, R. H., Hunter, W. C. and Noordergraaf, A. (1981). Functional consequences of expanded aortic bulb: a model study. *Am. J. Physiol.* **240**, R200-R210.

Coirault, C., Samuel, J. L., Chemla, D., Pourny, J. C., Lambert, F., Marotte, F. and Lecarpentier, Y. (1998). Increased compliance in diaphragm muscle of the cardiomyopathic Syrian hamster. *J. Appl. Physiol.* **85**, 1762-1769.

Conrad, W. A. (1969). Pressure–flow relationships in collapsible tubes. *IEEE Trans. Biomed. Eng.* **16**, 284-295.

Costidis, A. and Rommel, S. A. (2012). Vascularization of air sinuses and fat bodies in the head of the bottlenose dolphin (*Tursiops truncatus*): morphological implications on physiology. *Front Physiol* **3**, 243.

Cotten, P. B., Piscitelli, M. A., McLellan, W. A., Rommel, S. A., Dearolf, J. L. and Pabst, D. A. (2008). The gross morphology and histochemistry of respiratory muscles in bottlenose dolphins, *Tursiops truncatus. J. Morphol.* **269**, 1520-1538.

Cox, R. H. (1978). Passive mechanics and connective tissue composition of canine arteries. *Am. J. Physiol.* **234**, H533-H541.

Cozzi, B., Bagnoli, P., Acocella, F. and Costantino, M. L. (2005). Structure and biomechanical properties of the trachea of the striped dolphin *Stenella coeruleoalba*: evidence for evolutionary adaptations to diving. *Anat Rec A* **284**, 500-510.

Craig, A. B., Jr (1963). Heart rate responses to apneic underwater diving and to breath holding in man. *J. Appl. Physiol.* **18**, 854-862.

Dearolf, J. L. (2002). Morphology and development of the diaphragm of bottlenose dolphins (*Tursiops truncatus*). PhD thesis, Cornell University, Ithaca, NY.

Drabek, C. M. (1975). Some anatomical aspects of the cardiovascular system of Antarctic seals and their possible functional significance in diving. *J. Morphol.* **145**, 85-105.

Drabek, C. M. and Burns, J. M. (2002). Heart and aorta morphology of the deep-diving hooded seal (*Cystophora cristata*). *Can. J. Zool.* **80**, 2030-2036.

Fahlman, A., Hooker, S. K., Olszowka, A., Bostrom, B. L. and Jones, D. R. (2009). Estimating the effect of lung collapse and pulmonary shunt on gas exchange during breath-hold diving: the Scholander and Kooyman legacy. *Respir. Physiol. Neurobiol.* **165**, 28-39.

Falke, K. J., Busch, T., Hoffmann, O., Liggins, G. C., Liggins, J., Mohnhaupt, R., Roberts, J. D., Jr, Stanek, K. and Zapol, W. M. (2008). Breathing pattern, CO_2 elimination and the absence of exhaled NO in freely diving Weddell seals. *Respir. Physiol. Neurobiol.* **162**, 85-92.

Fung, Y. C. (1984). *Biodynamics Circulation*. New York: Springer-Verlag.

Gates, F., McCammond, D., Zingg, W. and Kunov, H. (1980). *In vivo* stiffness properties of the canine diaphragm muscle. *Med. Biol. Eng. Comput.* **18**, 625-632.

Goldbogen, J. A., Calambokidis, J., Shadwick, R. E., Oleson, E. M., McDonald, M. A. and Hildebrand, J. A. (2006). Kinematics of foraging dives and lunge-feeding in fin whales. *J. Exp. Biol.* **209**, 1231-1244.

Gosline, J. M. and Shadwick, R. E. (1996). The mechanical properties of fin whale arteries are explained by novel connective tissue designs. *J. Exp. Biol.* **199**, 985-997.

Griffiths, R. I., Shadwick, R. E. and Berger, P. J. (1992). Functional importance of a highly elastic ligament on the mammalian diaphragm. *Proc. R. Soc. B* **249**, 199-204.

Guppy, M., Hill, R. D., Schneider, R. C., Qvist, J., Liggins, G. C., Zapol, W. M. and Hochachka, P. W. (1986). Microcomputer-assisted metabolic studies of voluntary diving of Weddell seals. *Am. J. Physiol.* **250**, R175-R187.

Hui, C. A. (1975). Thoracic collapse as affected by the retia thoracica in the dolphin. *Respir. Physiol.* **25**, 63-70.

Humphrey, J. D. and DeLange, S. L. (2004). An introduction to biomechanics: solids and fluids, analysis and design. New York: Springer-Verlag.

Irving, L., Scholander, P. F. and Grinnell, S. W. (1942). The regulation of arterial blood pressure in the seal during diving. *Am. J. Physiol.* **135**, 0557-0566.

Jobsis, P. D., Ponganis, P. J. and Kooyman, G. L. (2001). Effects of training on forced submersion responses in harbor seals. *J. Exp. Biol.* **204**, 3877-3885.

Kooyman, G. L., Hammond, D. D. and Schroeder, J. P. (1970). Bronchograms and tracheograms of seals under pressure. *Science* **169**, 82-84.

Kooyman, G. L., Castellini, M. A. and Davis, R. W. (1981). Physiology of diving in marine mammals. *Annu. Rev. Physiol.* **43**, 343-356.

Laporta, D. and Grassino, A. (1985). Assessment of transdiaphragmatic pressure in humans. *J. Appl. Physiol.* **58**, 1469-1476.

Leith, D. E. (1976). Comparative mammalian respiratory mechanics. *Physiologist* **19**, 485-510.

Leith, D. and Lowe, R. (1972). Mechanics of baleen whale lungs. *Fed. Proc.* **31**, 335.

Lillie, M. A., Shadwick, R. E. and Gosline, J. M. (2010). Mechanical anisotropy of inflated elastic tissue from the pig aorta. *J. Biomech.* **43**, 2070-2078.

Lillie, M. A., Armstrong, T. E., Gérard, S. G., Shadwick, R. E. and Gosline, J. M. (2012). Contribution of elastin and collagen to the inflation response of the pig thoracic aorta: assessing elastin's role in mechanical homeostasis. *J. Biomech.* **45**, 2133-2141.

Lockyer, C. and Waters, T. (1986). Weights and anatomical measurements of northeastern Atlantic fin (*Balaenoptera-physalus*, Linnaeus) and sei (*Balaenoptera-borealis*, Lesson) whales. *Mar. Mamm. Sci.* **2**, 169-185.

Mcfarland, W. L., Jacobs, M. S. and Morgane, P. J. (1979). Blood-supply to the brain of the dolphin, *Tursiops truncatus*, with comparative observations on special aspects of the cerebrovascular supply of other vertebrates. *Neurosci. Biobehav. Rev.* **3 (Suppl. 1)**, 1-93.

Moore, M. J., Hammar, T., Arruda, J., Cramer, S., Dennison, S., Montie, E. and Fahlman, A. (2011). Hyperbaric computed tomographic measurement of lung compression in seals and dolphins. *J. Exp. Biol.* **214**, 2390-2397.

Mottishaw, P. D., Thornton, S. J. and Hochachka, P. W. (1999). The diving response mechanism and its surprising evolutionary path in seals and sea lions. *Am. Zool.* **39**, 434-450.

Murdaugh, H. V., Jr, Cross, C. E., Millen, J. E., Gee, J. B. L. and Robin, E. D. (1968). Dissociation of bradycardia and arterial constriction during diving in the seal *Phoca vitulina*. *Science* **162**, 364-365.

Nagel, E. L., Morgane, P. J., McFarlane, W. L. and Galliano, R. E. (1968). Rete mirabile of dolphin: its pressure-damping effect on cerebral circulation. *Science* **161**, 898-900.

Ninomiya, H., Inomata, T., Shirouzu, H. and Katsumata, E. (2005). Microanatomy of the terminal air spaces of Baird's beaked whale (*Berardius bairdii*) lungs. *J. Vet. Med. Sci.* **67**, 473-479.

Ommanney, F. D. (1932). The vascular networks (retia mirabilia) of the fin whale (*Balaenoptera physalus*). *Disc. Rep.* **5**, 327-362.

Patel, D. J., Janicki, J. S. and Carew, T. E. (1969). Static anisotropic elastic properties of the aorta in living dogs. *Circ. Res.* **25**, 765-779.

Pfeiffer, C. J. and Kinkead, T. P. (1990). Microanatomy of retia mirabilia of bowhead whale foramen magnum and mandibular foramen. *Acta Anat.* **139**, 141-150.

Piscitelli, M. A. (2009). Comparing thoracic morphology and lung size in shallow (*Tursiops truncatus*) and deep (*Kogia* spp.) diving cetaceans. MSc thesis, University of North Carolina Wilmington, Wilmington, NC, USA.

Piscitelli, M. A., McLellan, W. A., Rommel, S. A., Blum, J. E., Barco, S. G. and Pabst, D. A. (2010). Lung size and thoracic morphology in shallow- and deep-diving cetaceans. *J. Morphol.* **271**, 654-673.

Ponganis, P. J., Kooyman, G. L., Castellini, M. A., Ponganis, E. P. and Ponganis, K. V. (1993). Muscle temperature and swim velocity profiles during diving in a Weddell seal, *Leptonychotes weddellii. J. Exp. Biol.* **183**, 341-346.

Quick, C. M., Berger, D. S. and Noordergraaf, A. (1998). Apparent arterial compliance. *Am. J. Physiol.* **274**, H1393-H1403.

Quick, C. M., Berger, D. S., Stewart, R. H., Laine, G. A., Hartley, C. J. and Noordergraaf, A. (2006). Resolving the hemodynamic inverse problem. *IEEE Trans. Biomed. Eng.* **53**, 361-368.

Rhode, E. A., Elsner, R., Peterson, T. M., Campbell, K. B. and Spangler, W. (1986). Pressure-volume characteristics of aortas of harbor and Weddell seals. *Am. J. Physiol.* **251**, R174-R180.

Ridgway, S. H. and Howard, R. (1979). Dolphin lung collapse and intramuscular circulation during free diving: evidence from nitrogen washout. *Science* **206**, 1182-1183.

Ridgway, S. H., Scronce, B. L. and Kanwisher, J. (1969). Respiration and deep diving in the bottlenose porpoise. *Science* **166**, 1651-1654.

Rommel, S. A., Costidis, A. M., Fernández, A., Jepson, P. D., Pabst, D. A., McLellan, W. A., Houser, D. S., Cranford, T., vanHelden, A. L., Allen, D. M. et al. (2006). Elements of beaked whale anatomy and diving physiology and some hypothetical causes of sonar-related stranding. *J. Cetacean Res. Manag.* **7**, 189-209.

Scholander, P. (1940). Experimental investigations on the respiratory function in diving mammals and birds. *Hvalrådets skrifter* **22**, 1-131.

Shadwick, R. E. and Gosline, J. M. (1994). Arterial mechanics in the fin whale suggest a unique hemodynamic design. *Am. J. Physiol.* **267**, R805-R818.

Shadwick, R. E. and Gosline, J. M. (1995). Arterial Windkessels in marine mammals. *Symp. Soc. Exp. Biol.* **49**, 243-252.

Shardonofsky, F. R., Sato, J. and Bates, J. H. (1990). Quasi-static pressure-volume hysteresis in the canine respiratory system *in vivo*. *J. Appl. Physiol.* **68**, 2230-2236.

van Nie, C. J. (1987). Air-pressure in the thoracic cavity of the deep diving whale (a theoretical biomechanical approach). *Aquat. Mamm.* **13**, 23-25.

Vogl, A. W. and Fisher, H. D. (1982). Arterial retia related to supply of the central nervous system in two small toothed whales – narwhal (*Monodon monoceros*) and beluga (*Delphinapterus leucas*). *J. Morphol.* **174**, 41-56.

Vogl, A. W., Todd, M. E. and Fisher, H. D. (1981). An ultrastructural and fluorescence histochemical investigation of the innervation of retial arteries in *Monodon monoceros*. *J. Morphol.* **168**, 109-119.

Walmsley, R. (1938). Some observations on the vascular system of a female fetal finback. *Contrib. Embryol.* **27**, 107-178.

Westerhof, N., Lankhaar, J. W. and Westerhof, B. E. (2009). The arterial Windkessel. *Med. Biol. Eng. Comput.* **47**, 131-141.

Yablokov, A. V., Bel'kovich, V. M. and Borisov, V. I. (1974). *Whales and Dolphins*. Arlington, VA: Joint Publications Research Service.

Young, I. S., Alexander, R. M., Woakes, A. J., Butler, P. J. and Anderson, L. (1992). The synchronization of ventilation and locomotion in horses (*Equus caballus*). *J. Exp. Biol.* **166**, 19-31.

Yu, Q., Zhou, J. and Fung, Y. C. (1993). Neutral axis location in bending and Young's modulus of different layers of arterial wall. *Am. J. Physiol.* **265**, H52-H60.

Zapol, W. M., Liggins, G. C., Schneider, R. C., Qvist, J., Snider, M. T., Creasy, R. K. and Hochachka, P. W. (1979). Regional blood flow during simulated diving in the conscious Weddell seal. *J. Appl. Physiol.* **47**, 968-973.